REVIEW ARTICLE

Transition between nuclear and quark–gluon descriptions of hadrons and light nuclei

Rep. Prog. Phys. **75** (2012) 086301 (24pp) doi:10.1088/0034-4885/75/8/086301

Transition between nuclear and quark–gluon descriptions of hadrons and light nuclei

R J Holt[1] **and R Gilman**[2]

[1] Physics Division, Argonne National Laboratory, Argonne, IL 60439, USA
[2] Department of Physics, Rutgers University, Piscataway, NJ 08854, USA

E-mail: holt@anl.gov and gilman@jlab.org

Received 17 October 2011, in final form 25 May 2012
Published 26 July 2012
Online at stacks.iop.org/RoPP/75/086301

Abstract
We provide a perspective on studies aimed at observing the transition between hadronic and quark–gluonic descriptions of reactions involving light nuclei. We begin by summarizing the results for relatively simple reactions such as the pion form factor and the neutral pion transition form factor as well as that for the nucleon and end with exclusive photoreactions in our simplest nuclei. A particular focus will be on reactions involving the deuteron. It is noted that a firm understanding of these issues is essential for unravelling important structure information from processes such as deeply virtual Compton scattering as well as deeply virtual meson production. The connection to exotic phenomena such as color transparency will be discussed. A number of outstanding challenges will require new experiments at modern facilities on the horizon as well as further theoretical developments.

(Some figures may appear in colour only in the online journal)

This article was invited by G Baym.

Contents

1. Introduction

One of the central goals of nuclear physics is the description of hadrons and nuclei at a truly fundamental level. While quantum chromodynamics (QCD) is the theory of the strong interaction, making use of this theory is one of the most challenging endeavors in science. The problem is that non-perturbative methods must be used to describe the real world. Observables are controlled by two emergent phenomena: confinement and dynamical chiral symmetry breaking (DCSB). DCSB is responsible for more than 98% of the visible mass in the Universe. The effect of DCSB has been studied through lattice calculations [1], the Dyson–Schwinger equation (DSE) approach [2, 3], as well as instanton

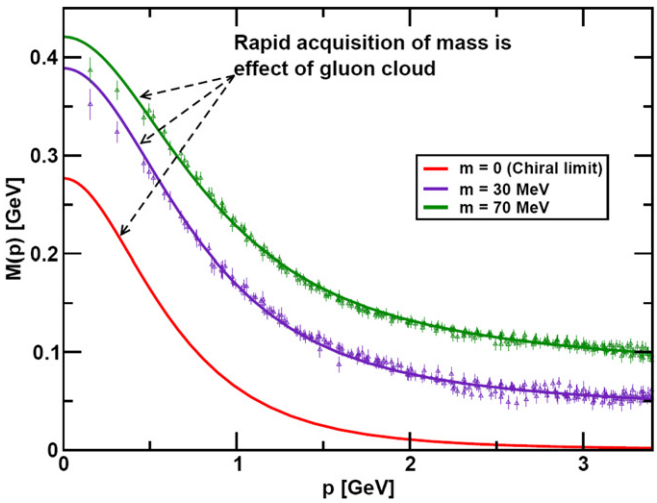

Figure 1. DSE calculations of quark mass as a function of the magnitude of the dressed quark's four momentum for several current quark masses, as denoted by m. The points with error bars are from lattice QCD calculations. The solid red curve is the result for a vanishing current quark mass, the chiral limit. Reproduced with permission from [11]. Copyright 2008 Elsevier.

models [4]. The results of these calculations are shown in figure 1. In this figure the mass of the quark is plotted as a function of the magnitude of the dressed quark's four momentum. Clearly as the quark momentum increases to 2 GeV and beyond, the quark mass has fallen rapidly from its constituent quark mass to nearly its current quark mass. Even under the assumption of perfect chiral symmetry, i.e. a vanishing quark mass as given by the solid red line in the figure, the quark mass evolves to essentially the constituent quark mass at low momentum. In future experiments, it will be interesting to determine how this rapid change in quark mass can affect high-energy nuclear reactions. The interesting regions will be reactions in kinematic regimes where the quark mass function changes rapidly.

One approach to our understanding of hadrons at this fundamental level is to determine the role of the quarks and gluons in hadronic and nuclear reactions. In particular, determining whether there is a clean transition from hadronic to quark–gluon degrees of freedom has been an important pursuit both experimentally and theoretically. Historically, the constituent counting rule [5–7], hadron helicity conservation [8] and color transparency (CT) effects [9] have often been cited as evidence for the underlying quark degrees of freedom in reactions. The constituent counting rule states that the cross-section, $d\sigma/dt$, should have a simple power law behavior based on the number of constituents, n, involved in the process: $d\sigma/dt \sim s^{2-n}$ where s and t are the usual Mandelstam variables. Many experimental studies (see [10] for an example) of exclusive reactions at high energies are consistent with the constituent counting rules. It is believed that these effects should become manifest when perturbative QCD (pQCD) is valid. In recent years, understanding exactly where pQCD and non-pQCD are dominant has become important for studies of structure functions, the generalized parton distribution functions (GPDs), which provide information on quark position–momentum correlations, in particular. For example, the exclusive processes of deeply virtual Compton scattering (VCS) and deeply virtual meson production have been put forward as reactions necessary to isolate features of the GPDs, and depend on the process being factorizable into a hard production process and soft hadronic structure.

Intertwined with the idea of a quark–hadron transition is the idea of duality. Bloom and Gilman [12] introduced the idea, finding that an average over the resonance region in inelastic electron scattering is equivalent to the scaling curve in deep-inelastic scattering, and thus to quark behavior. Duality has been a ongoing topic of a number of experimental and theoretical investigations, including extension from inclusive electron scattering to a variety of other reactions—for an extensive review, see [13]. A recent example of an experimental investigation [14] of duality is in semi-inclusive pion production reactions. While the idea of duality in the case of the nucleon is generally accepted, there is controversy over whether hadronic and quark degrees of freedom are equivalent when considering the NN force and nuclear structure, as will be discussed in section 2.

In this report, we will present highlights from the vast body of data aimed at discovering the transition from the hadronic picture, which is well accepted at low energy, to the QCD picture, which is the theory of the strong interaction. The evidence is overwhelming that pQCD scaling is not achieved, except in the simplest systems, in exclusive reactions at contemporary kinematics. Here, we focus on the form factors and transition form factors of the pion, nucleon and deuteron as well as photodisintegration of the nucleon, deuteron and ^{3}He. In addition, we will review the evidence for the CT effect which is believed to be a necessary precursor for factorization in semi-exclusive reactions. In particular, we discuss results for high-energy exclusive reactions from Stanford Linear Accelerator Center (SLAC), Jefferson Lab (JLab), Fermi National Accelerator Laboratory (FNAL) and Brookhaven National Laboratory (BNL). On the theoretical side the challenge is to calculate the kinematic dependences of the form factors, transition form factors and reaction cross-sections for simple systems. Here we summarize the contemporary issues and approaches in the field.

2. Quark–gluon versus hadronic descriptions at low energy

Quarks and gluons, the degrees of freedom of QCD, are confined within hadrons, the degrees of freedom that are detected by experiments. Thus it seems obvious that in principle equivalent descriptions can be formulated in terms either of quark and gluon or of hadronic basis states. This viewpoint has, however, been challenged by some theorists, since the early days of QCD and quark theories [15]. Here we will give examples of three such arguments. However this argument is resolved, it remains a practical question whether it is possible to formulate a satisfactory theoretical description with either set or both sets of basis states.

From the quark-model point of view, it should be pointed out that six-quark systems having the same quantum numbers

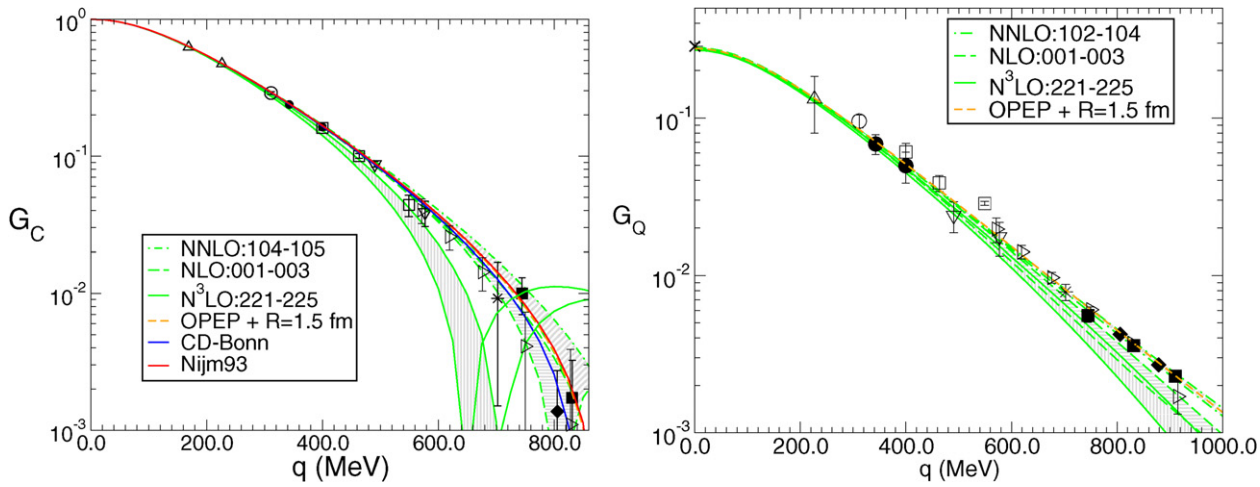

Figure 2. The charge (left) and quadrupole (right) form factors of the deuteron in χPT. Reproduced with permission from [33].

as baryon–baryon systems will in part have configurations that do not break down into individual baryon quantum numbers [16–18]. The deuteron-like 6-quark wave function has the form

$$\psi = \sqrt{1/9}\,\psi_{\rm NN} + \sqrt{4/45}\,\psi_{\Delta\Delta} + \sqrt{4/5}\,\psi_{\rm CC}, \qquad (1)$$

where the final CC component is a non-baryonic hidden-color component—two three-quark systems, each with net color, that add to a colorless deuteron. The argument is that the hidden-color component of the wave function cannot be represented by colorless hadrons. However, a nonrelativistic constituent quark-model calculation [19] found that there is a strong dynamical clustering of the six-quark system into an NN configuration, with a strong repulsive core to the NN interaction. This suggests that the hidden-color component of the NN wave function is strongly suppressed for low-energy phenomena.

A second argument arises from the quark–meson coupling model applied to nucleons in nuclei [20]. In this viewpoint it is unsurprising to find that nucleon structure is modified by the nucleon being placed in a strong external field. Since the model leads to an effective interaction in nuclei that agrees well with the phenomenological Skyrme force, it supports the idea that one should think of nuclei as made up of quasi-particle nucleons, as opposed to free nucleons.

An additional argument arises from a consideration of confinement [21]. Ralston argues that hadrons are incomplete to describe their own interactions, when color is exchanged. The system cannot be required to be colorless at all times, so '*there is not supposed to be a local effective hadronic theory of any kind representing QCD.*'

If these objections are valid, one might view lattice QCD or a Dyson–Schwinger approach as the only theoretically acceptable solutions at present to low-energy QCD. However, lattice QCD remains limited by computational capabilities, with only some initial steps taken in exploring the NN force. Thus, even if these arguments are valid, we anticipate that QCD inspired effective hadronic field theories will remain a basis for our understanding low-energy QCD for many years.

2.1. Effective field theories

A number of theories related to QCD have been developed to describe nonperturbative, low-energy phenomena. Here we briefly describe Skyrme theory, pionless effective field theory, EFT($\not\pi$), and chiral perturbation theory, χPT.

Skyrme theory [22] treats baryons as topological solitons of an effective pion theory, justified by the large N_c limit in which QCD becomes a theory of mesons [23]. The theory has been applied to baryons, NN interactions [24], the structure of the deuteron—see [25] for a review of and references to earlier work, and more recently even to α particles [26] and neutron stars [27]. Predictions tend to be qualitatively rather than quantitatively correct.

Modern EFT($\not\pi$) was developed first by Weinberg [28]. The idea is that the physics at lower momentum than a scale m_π can be described with an expansion in powers of p/m_π that reflects all desired symmetries. There remain issues and subtleties with implementing the theory—see [29–31] for further discussion. In EFT($\not\pi$), NN interactions arise from contact terms. An example of the structure of the deuteron in EFT($\not\pi$) is [32]. The calculation quantitatively describes the deuteron form factors only up to $Q^2 \approx m_\pi^2$, about as expected. In this approach the well-known issue of calculating the correct value for the deuteron quadrupole moment is solved by fixing the constant of a short-distance term involving a four-nucleon, one-photon contact term.

Using an expansion scale of m_ρ adds pions to the EFT, leading to χPT. Calculations of the NN force are now up to fourth order, and describe NN phase shifts well up to 250 MeV. Earlier more qualitative predictions of the deuteron electromagnetic form factors, such as [34], have led to excellent quantitative predictions [33] up to about $Q \approx m_\rho$, as shown in figure 2. See sections 5.1 and 5.2 for discussion of the deuteron structure at higher Q^2.

2.2. The issue of medium modifications

At the beginning of this section we discussed the issue of hadronic versus quark–gluon theories. When nucleons within nuclei are studied, the question arises whether the properties

of the nucleon are changed. One viewpoint is that when a composite quark system, the nucleon, is subjected to the strong external nuclear force, the properties of the system are modified. The alternate viewpoint is that we have a many-body system of interacting hadrons, which can be described in terms of the properties and interactions of the free hadrons. These two viewpoints are related to the degrees of freedom used, and might ultimately be different ways of looking at the same physics, leading to equivalent predictions. Even if the theories are not in principle equivalent, since hadronic theories are based on the measured NN force, any quark effects may be in part effectively accommodated by the hadronic theory. In practice, the issue is whether observables are more simply predicted from theories that incorporate quark-model inspired medium modifications, or whether observables are well understood from hadronic theories without medium modifications. Experimentally, this issue has been addressed by experiments concerning the Coulomb sum rule, quasi-free electron scattering, polarization transfer to nucleons in nuclei and deep-inelastic scattering on nuclei and the EMC effect.

2.2.1. Coulomb sum rule. Inclusive (e, e′) scattering can be described as a sum of two response functions, the transverse and longitudinal response functions $R_T(\vec{q},\omega)$ and $R_L(\vec{q},\omega)$, respectively. Here $\vec{q}$ and ω are the momentum and energy transfer. The transverse (longitudinal) function R_T (R_L) corresponds to virtual photons with transverse (longitudinal) electromagnetic fields like (unlike) the real photon, and reflects the magnetic (electric) structure of the target. Following [35], the Coulomb sum rule can be defined as

$$S_L(\vec{q}) = \frac{1}{Z}\int_{\omega_0}^{\infty} \frac{R_L(\vec{q},\omega)}{\tilde{G}_E^2}\,\mathrm{d}\omega, \qquad (2)$$

where $\tilde{G}_E^2 = G_{Ep}^2 + N/Z\, G_{En}^2$ and ω_0 is the inelastic threshold. Ignoring the neutron contributions, the integral in S_L may be thought of as counting the number of protons in the nucleus. At low $\vec{q}$, below a few hundred MeV/c, nucleon correlations reduce the sum rule below unity, but it is believed that by about 500 MeV/c, deviations of the sum rule from unity would be indicative of medium modifications. The experimental status of the Coulomb sum rule might be regarded as not yet clear, due to conflicting analyses of the world data—see [35] for a discussion. While recent theoretical work [36] on Coulomb corrections, a major issue in the analyses, appears to support the idea that the Coulomb sum rule is quenched, the uncertainties are not sufficient for a definite conclusion. The situation should be improved in the near future due to a recent JLab experiment [37].

2.2.2. Quasi-free electron scattering. In the impulse approximation, the shape of the quasi-free scattering peak reflects the momentum distribution of nucleons in nuclei, while its magnitude reflects the nucleon form factors. Thus cross-sections from different kinematics, and even from different nuclei, can be checked for consistency with free nucleon form factors. This is most often performed with cross-sections rescaled by a scaling function to follow a universal curve. Most familiar is probably y scaling, but there is also ξ scaling, or superscaling with ψ'. As discussed in [35], this technique has largely been used to set limits on medium modifications of below ≈3%; the limit is sensitive mostly to the magnetic form factor.

2.2.3. Polarization transfer to nucleons in nuclei. The $\vec{\mathrm{e}}\mathrm{p} \to \mathrm{e}'\vec{\mathrm{p}}$ polarization transfer reaction determines the proton form factor ratio through

$$\frac{G_E}{G_M} = -\frac{E+E'}{2M}\cot\frac{\theta}{2}\,\frac{P_x}{P_z}, \qquad (3)$$

where $P_{x,z}$ are polarization components of the final-state proton, E (E') is the initial (final) state electron energy, M is the nucleon mass, and θ is the electron scattering angle. For protons in nuclei, the same ratio can be determined, although the identification of this ratio with an in-medium form factor ratio is suspect at best; formally there are six half-off-shell proton form factors. The most recent experimental work [38] reaffirmed with improved uncertainties that the proton polarization ratio is reduced by about 10% for protons ejected from ^{4}He—see figure 3.

This reduction in the ratio has been explained by two calculations. First, calculations by the Madrid group [41] are unable to reproduce the ratio without including medium modified nucleon form factors. The quark–meson coupling (QMC) modifications in figure 3 are from [42], while the chiral quark soliton (CQS) modifications are from [43]; both models lead to similar results. The QMC model of the nucleon uses constituent quarks confined in a nucleon, with nucleons interacting through pions exchanged between quarks. The CQS model of the nucleon is based on instantons in large N_c QCD and DCSB, and includes sea quarks absent in the QMC approach. The validity of the idea of medium modifications is supported by a suggestion from [44], that medium modifications for low momentum should increase with the nucleon virtuality; the right panel of figure 3 intriguingly shows such an effect.

Secondly, a conventional nuclear physics explanation is given by [45] in a much more detailed calculation that includes meson-exchange currents (MECs), tensor correlations and spin-dependent and independent charge-exchange final-state interactions. While the calculation of [41] arguably is very simplistic, the calculation of [45] can be criticized as not entirely constrained by data from other reactions. The induced polarization in $^4\mathrm{He}(\mathrm{e},\mathrm{e}'\mathrm{p})^3\mathrm{H}$ *suggests* that the final-state interactions in [45] are very strong, but the result is not definitive.

Thus, the correct interpretation of the polarization transfer reactions appears inconclusive. The next step in resolving this issue will likely come from the interesting theoretical result of [46]. A model-independent prediction is that, while the form factor ratio in the proton is expected to decrease, the form factor ratio in the neutron is expected to increase. As an experiment at JLab in the 12 GeV era appears unfeasible due

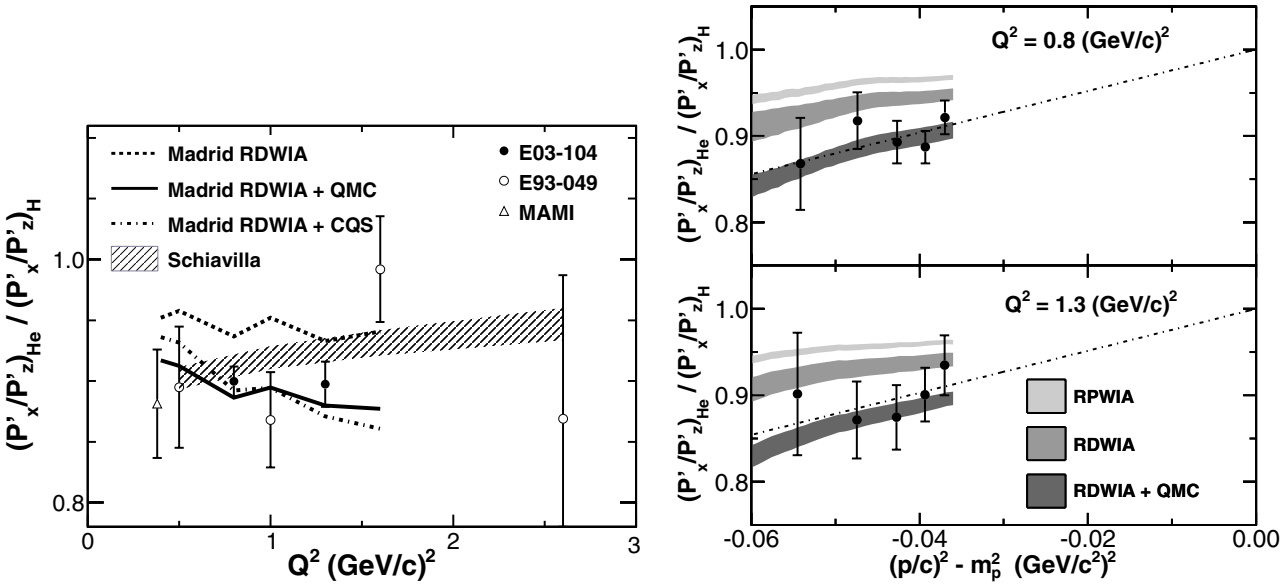

Figure 3. The ratio of transverse to longitudinal polarization components of a proton ejected from ^{4}He compared with a free proton. The left panel is integrated over the full acceptance, while the right panel is for each of the E03-104 Q^2 points of [38] as a function of the initial-state proton virtuality. The Mainz Microtron (MAMI) point is from [39], the E93-049 points are from [40]. Curves are described in the text. Adapted from [38].

to the high beam energies, an experiment is being developed for MAMI at Mainz.

2.2.4. EMC effect. The origins of the EMC effect [47], the depletion of quark distributions in nuclei at moderate Bjorken x, remain ambiguous nearly 30 years after the effect was first observed. A number of experiments have confirmed the depletion seen in the EMC results, and it is generally accepted that the explanation must lie in a modification of the quark distribution of nucleons. In [48], it was argued that the EMC effect could not be explained on the basis of a nucleon-only model of the nucleus, and that constraints on antiquarks in nuclei are inconsistent with explaining the EMC effect within a nucleon + meson model of nuclei. There have been interesting attempts to explain the EMC effect based on many-body theory [49, 50]. Although these approaches have not been ruled out, there is substantially more work necessary to successfully describe the effect without resorting to partonic descriptions.

Deep-inelastic scattering from light nuclei is a particularly powerful approach to study medium modifications since realistic nuclear calculations can be performed and since Coulomb effects [51] are minimized. Recent measurements in light nuclei [52] appear to show that the EMC effect correlates more with local density, for example alpha clusters in ^{9}Be, than with average nuclear density. Also, a recent analysis [53] indicates a correlation between the strength of the EMC effect and the strength of short-range correlations in nuclei. However, these clues do not uniquely identify the underlying dynamics. New measurements that will provide helpful information include improved measurements of the EMC effect in the Drell–Yan process [54], studies of quark-flavor dependence in the EMC effect, a measurement of the EMC effect in the triton [55], and a possible spin-dependence in the EMC effect [56].

3. Transition from hadronic to quark–gluon degrees of freedom

3.1. The pion

3.1.1. The pion elastic form factor. The pion elastic form factor is very interesting since non-perturbative calculations can be performed for this relatively simple system. In addition, the asymptotic limit[3] at infinitely high Q^2 is known [57, 58] and is given by

$$F_\pi(Q^2) \overset{Q^2\to\infty}{\longrightarrow} \frac{16\pi\alpha_s(Q^2)f_\pi^2}{Q^2}, \tag{4}$$

where α_s is the strong coupling constant and f_π is the pion decay constant. The Q^2 dependence of this form factor is consistent with the constituent counting rule for electron elastic scattering from the pion. An interesting way to gauge the transition region between hadronic and partonic degrees of freedom might be from the quark mass itself. Theoretical studies [59] of the pion form factor indicate that the running of the quark mass is an important ingredient in the calculations. We know that Bjorken scaling [60–62] sets in at relatively low values of momentum transfer in deep-inelastic scattering, i.e. when more than $\approx$2 GeV/c is imparted to the quark. From figure 1 it is noted that the quark mass is already near its current quark mass at 2 GeV/c. The pion form factor presents an interesting test case since the pion is only a quark–antiquark system. To impart an average of 2 GeV/c to a quark and antiquark, only 16 GeV^2 need be imparted to the pion. This should be achievable or nearly achievable in both the space-like and time-like regions, defined in figure 4. Note that for time-like momentum transfers, this argument is

[3] As we focus on space-like momentum transfers, we follow the convention that $-q^2 = Q^2 > 0$.

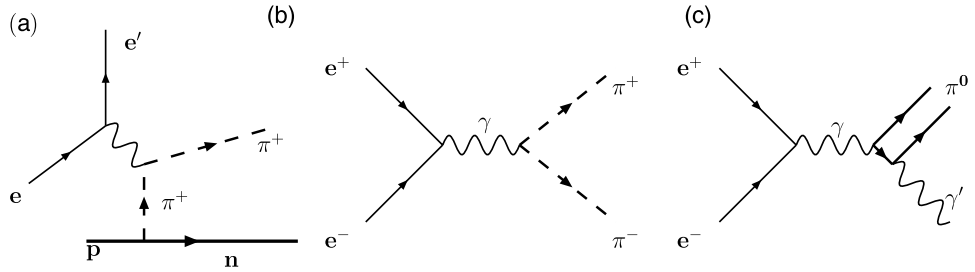

Figure 4. Diagrams of (*a*) electron scattering from a virtual pion in a proton, (*b*) the $e^+e^- \to \gamma^* \to \pi^+\pi^-$ reaction, and (*c*) the $e^+e^- \to \gamma^* \to \pi^\circ e^+e^-$ reaction.

invalid in regions where high-mass resonances modify the form factor. The space-like data at very high Q^2 make use of the process indicated in figure 4(*a*), i.e. electron scattering from the virtual pion cloud in the proton. Time-like data are from the process in figure 4(*b*), where the $e^+e^- \to \gamma^* \to \pi^+\pi^-$ reaction is employed. Existing precision data in the space-like region [63–68] and a sample of data in the time-like region [69] for the pion elastic form factor are shown in figure 5. Three disparate theoretical approaches [70–72] are also represented in the figure. The DSE calculations should approach the pQCD limit at very high-momentum transfer, while the AdS/QCD approach will give at least the same Q^2 dependence. (AdS/QCD attempts to solve the strong coupling theory of QCD with the string-theory inspired technique of solving a dual theory with weak coupling in five-dimensional space. See, e.g., [73].) For an informative review of the space-like form factor data, see [68] and for an excellent theoretical review, see [71, 74].

At very low values of Q^2, the form factor was measured [63–65] by scattering real pions from electrons in a target. However, at high values of Q^2, the pion space-like form factor is deduced from electron scattering from a virtual pion in a proton target. Highly precise data [66–68, 75] have been taken only up to a momentum transfer of 2.5 GeV^2 at Jefferson Lab. When the JLab facility is upgraded to 12 GeV, data up to 6 GeV^2, where the hard and soft processes become comparable, should be possible. Currently, two high Q^2 values for the time-like pion form factor have been reported [76, 77] at 9.6 and 13.48 GeV^2. Although one might expect that pQCD would begin to dominate at these values of momentum transfer, the results are $Q^2F_\pi = 0.94 \pm 0.08$ and $1.01 \pm 0.11 \pm 0.07$ GeV^2, respectively, much larger than the value of $\approx$0.10 GeV^2 expected for pQCD as given by (4); the predictions for space-like and time-like form factors should be similar. The large value of the time-like form factor indicates that the process is primarily non-perturbative or that resonances have a strong influence even at this high value of q^2. The prospect for improving the measurements in the time-like region is excellent because of the e^+e^- colliders in operation or recently in operation.

3.1.2. Pion transition form factor. The lowest order diagram that describes the $e^+e^- \to e^+e^-\pi^\circ$ process is shown in figure 4(*c*). The pion transition form factor in lowest order pQCD can be determined from

$$Q^2F_{\pi\gamma}(Q^2) = \frac{\sqrt{2}f_\pi}{3}\int_0^1 \frac{\mathrm{d}x}{x}\phi_\pi(x, Q^2), \tag{5}$$

where f_π is the pion decay constant, x is the momentum fraction for a parton in the pion and ϕ_π is the parton distribution amplitude for a parton in the pion. The pion transition form factor has traditionally been cited as the best example of the approach to a pQCD limit. The process has an asymptotic limit [78] that is much larger than that of the pion form factor:

$$Q^2F_{\pi\gamma}(Q^2) \overset{Q^2\to\infty}{\longrightarrow} \sqrt{2}f_\pi. \tag{6}$$

Recent results [79, 80] from the BaBar Collaboration for the $e^+e^- \to e^+e^-\pi^\circ$ process have been extended to a Q^2 of $\approx$40 GeV^2 and surprisingly these results do not exhibit a Q^{-2} dependence for the form factor expected from pQCD. Nevertheless, some authors [81–84] have described the data by using QCD-inspired models. Recent works [85, 86] argue strongly that reasonable nonperturbative descriptions of this process should approach the pQCD limit from below the limit, a perspective also developed elsewhere [87–90]. These results appear to cast doubt on the data which exceed the limit at such high values of Q^2. Moreover, recent BABAR data [91, 92] for the transition form factors of the η, η' and η_c appear to be described by pQCD treatments at high Q^2. Recent data from the Belle Collaboration [93] are below the BaBar result, more consistent with the high Q^2 asymptotic limit.

3.2. The nucleon

3.2.1. Elastic form factors. A recent review of the electromagnetic nucleon form factors is [94]. Here we focus on the high Q^2 behavior of the form factors. We consider the helicity-conserving Dirac F_1 and helicity-nonconserving Pauli F_2 form factors, or equivalently the electric and magnetic form factors, $G_E = F_1 - \tau F_2$ and $G_M = F_1 + F_2$, respectively, with $\tau = Q^2/4m_p^2$. Ignoring logarithmic corrections and running of the strong coupling constant $\alpha_s(Q^2)$, the constituent counting rules and pQCD [78] predict that F_1 falls as $1/Q^4$, and F_2 falls as $1/Q^6$, so G_M also falls as $1/Q^4$. While the magnitudes of the form factors at $Q^2 \to \infty$ are not known, with reasonable assumptions $G_M^n/G_M^p \to -2/3$. Following our arguments above, one might expect that the proton form factors become asymptotic for $Q^2 \approx 36$ GeV^2.

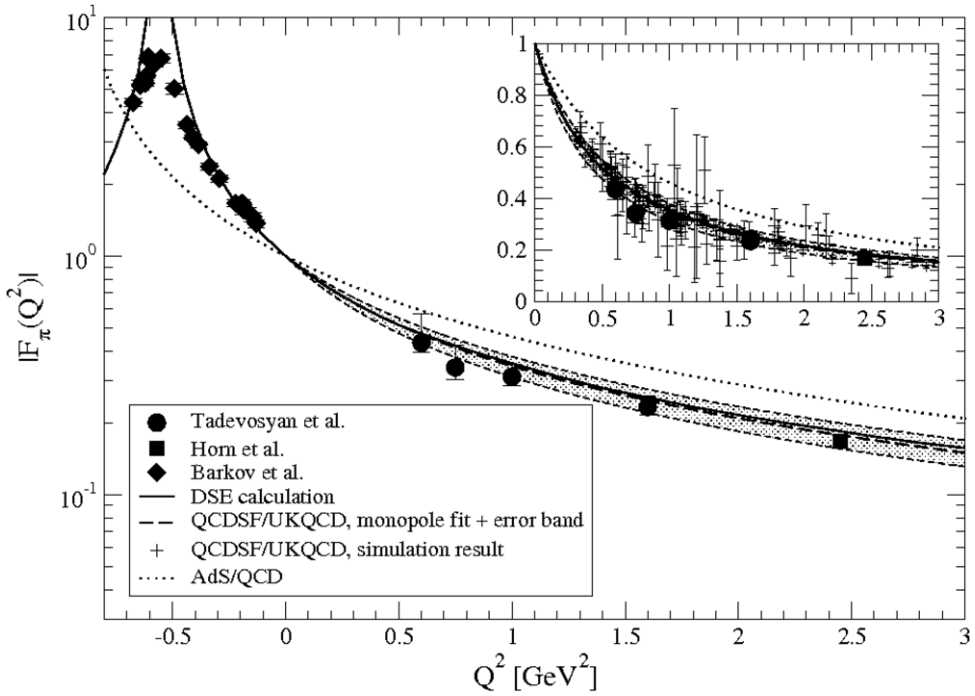

Figure 5. Pion form factor data in both the space- and time-like regions. The three curves represent the DSE calculation (solid), the AdS/QCD calculation (dotted) and the lattice QCD calculations (shaded region). Reproduced with permission from [71].

To date, the ranges of measurements for the various form factors are limited to $Q^2 \approx 30\,\mathrm{GeV}^2$ for G_M^{p} [95], $5\,\mathrm{GeV}^2$ for G_M^{n} [96], $8.5\,\mathrm{GeV}^2$ for G_E^{p} [97] and $3.4\,\mathrm{GeV}^2$ for G_E^{n} [98], so one should not expect perturbative form factor behavior. However both magnetic form factors follow the dipole formula, $G_M^{\mathrm{p,n}} = \mu_{\mathrm{p,n}} G_D = (1 + Q^2/0.71)^{-2}$, which has the expected high-Q^2 scaling, within about 10%. Furthermore, with similar precision, at all Q^2 $G_M^{\mathrm{n}}/G_M^{\mathrm{p}} \approx \mu_{\mathrm{n}}/\mu_{\mathrm{p}} = -0.685$, which is consistent with the predicted ratio of $-2/3$. In contrast, estimates of the actual magnitude of the perturbative QCD contribution to the proton magnetic form factor [99] indicate that it is likely small, perhaps 1% of G_M^{p}.

The electric form factors do not follow the dipole formula; the falloff of $G_E^{\mathrm{p}}(Q^2)/G_D(Q^2)$ is well known—this disagrees with the scaling expectation [5] that $G_E/G_M \rightarrow$ constant. We consider instead the ratio F_2/F_1. Using $R = G_E/G_M$, $F_2/F_1 = (1 - R)/\kappa(\tau + R)$. (We normalize $G_M(0) = \mu$ but $F_2(0) = 1$.) In pQCD, neglecting orbital angular momentum contributions, helicity flip costs a power of Q^2 so that one expects $Q^2 F_2/F_1 \rightarrow$ constant. But since the first JLab G_E^{p} data appeared [100] it has been known that this formula does not work well in the range of measured data; instead $QF_2/F_1 \approx$ constant. This result was explained with quark models as indicating the importance of relativity and orbital angular momentum of the quarks in the proton [101]. A refined pQCD analysis including orbital angular momentum suggests a modified scaling, $Q^2 F_2/F_1 \propto \ln^2(Q^2/\Lambda^2)$, with Λ a constant [102]. (See also [103].) Figure 6 shows that this formula works quite well for the proton, but it does not work at all for the neutron. The Dyson–Schwinger calculation, drawn from [104–106], has been extended up to $12\,\mathrm{GeV}^2$ for the first time as shown in figure 6. The agreement up to $5\,\mathrm{GeV}^2$ is quite good, but the deviation from the data for the proton is dramatic. A possible refinement to this calculation is to choose a quark mass function (see figure 1) that has a different falloff rate for the quark momentum; the ratio might be a sensitive probe of the momentum dependence of the dressed quark mass function.

Of equal importance to the space-like form factors measured with electron scattering are the time-like form factors measured in colliders through reactions such as $\mathrm{p\bar{p}} \rightarrow \mathrm{e^+e^-}$. The cross-section is given by

$$\frac{\mathrm{d}\sigma}{\mathrm{d}\Omega} = \frac{\alpha^2}{2s\sqrt{1 - 4m_{\mathrm{p}}^2/s}} \times \left[(1 + \cos^2\theta) G_M^2(s) + \frac{4m_{\mathrm{p}}^2}{s} \sin^2\theta G_E^2(s) \right], \tag{7}$$

where θ is the outgoing electron angle and Mandelstam $s = q^2 = -Q^2$ is the photon virtuality.

While it might appear that the differing angle dependences of the electric and magnetic terms make separations easy, the low luminosity of experiments coupled with small cross sections and large backgrounds has in general prevented separation of G_E and G_M. Instead it is typically assumed either that $G_E = 0$ or $G_E = G_M$. The estimated time-like proton magnetic form factor for $q^2 > 8\,\mathrm{GeV}^2$ appears to roughly scale as expected from pQCD, with $q^4 G_M \propto \alpha_{\mathrm{strong}}^2$. However, from pQCD it is expected that $G_{M\,\text{time-like}}(q^2) = G_{M\,\text{space-like}}(Q^2)$, while experimentally the time-like form factor is about a factor of two larger.

To summarize, even though existing data are not expected to be in the perturbative regime, the magnetic form factors agree reasonably well with the expected pQCD scaling. The proton form factor ratio can be considered to be in agreement as well, if orbital angular momentum is included. The

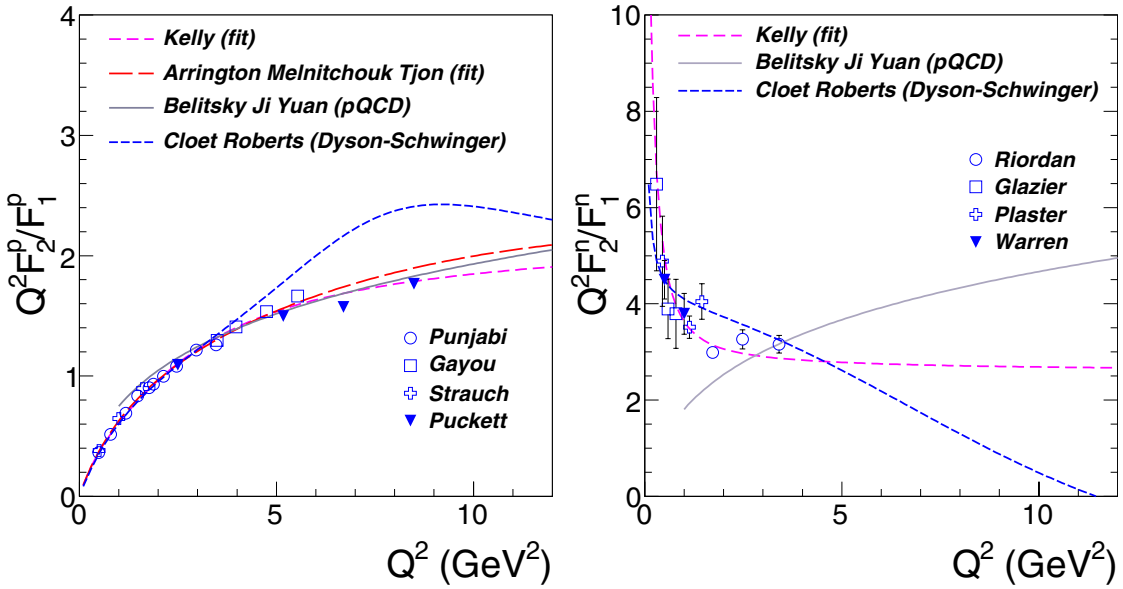

Figure 6. The form factor ratio Q^2F_2/F_1 for a restricted set of data for the proton (left) and the neutron (right) compared with the Kelly fit [107], the 'AMT' fit for the proton [108], a recent Dyson–Schwinger calculation [104–106], and the 'BJY' pQCD scaling function from [102] with $\Lambda = 0.15$ GeV, normalized to the higher Q^2 data. Increasing Λ to 0.20 GeV would basically overlap the AMT fit, while decreasing Λ to 0.10 GeV would basically overlap the Kelly fit. The 'BJY' parameterization cannot work for the neutron unless the ratio increases. Data are from Punjabi *et al* [109], Gayou *et al* [110], Strauch *et al* [40], Puckett *et al* [97], Riordan *et al* [98], Glazier *et al* [111], Plaster *et al* [112], and Warren *et al* [113].

neutron electric form factor does not agree with perturbative expectations, nor does the ratio of time-like to space-like form factors. Since the form factor magnitudes appear to be largely nonperturbative, the agreements in the scaling behavior might be fortuitous. While it is beyond our scope to address in any detail, the form factor data can be qualitatively understood through various quark models or parameterized GPDs.

3.2.2. Hard Compton scattering at high energy. The real Compton scattering (RCS) reaction is $\gamma p \to \gamma p$. The pQCD prediction for hard (Mandelstam s, $-t$, and $-u \gg m_p^2$) RCS is $d\sigma/dt\,(\theta_{cm}) \propto s^{-6}$. As shown in figure 7, this prediction was roughly supported by cross-section data from Cornell [114] for $E_\gamma = 2$–6 GeV, but a subsequent more comprehensive Jefferson Lab experiment [115] found the scaling is more consistent with s^{-8}; oddly both experiments find s^{-7} scaling at $\theta_{cm} = 90^\circ$. Differences between the two results could be explained if there were an energy-dependent leakage of $\gamma p \to p\pi^0$ events into the RCS channel in the Cornell data, as π^0 production is about two orders of magnitude larger at these energies.

The most recent pQCD calculation of RCS is given in [117], which reviews and compares with earlier work. A sample Feynman diagram is shown in figure 8. If the RCS calculation is normalized using the ratio to the proton form factor, then the RCS calculations are only a factor of several below the data; the factor decreases with energy due to the faster energy dependence of the data. Polarization transfer coefficients were measured in [116], see figure 7, but for $E_\gamma = 3$ GeV and $\theta_{cm} = 120^\circ$, corresponding to Mandelstam $-u = 1.1$ GeV^2, which is too small to expect pQCD to apply.

There have been several attempts to describe RCS through the handbag mechanism, shown in figure 8, such as in a constituent quark model [118] and with GPDs [119, 120], in which RCS depends on $1/x$ moments of the GPDs. While the validity of factorization in the GPD approach to real photon reactions has been questioned, it is addressed in [119, 120]. Generally, there has been sufficient flexibility in these approaches to at least qualitatively, but consistently explain the nucleon form factor and RCS data. There appears to be no simple explanation[4] of why the scaling has $n = 8$. These approaches also explain the polarization transfer measurement. While these model calculations for the polarization transfer tend to qualitatively resemble the Klein–Nishina result, as shown in figure 7, apparently the interferences between various diagrams in the pQCD calculations lead to the full calculation being very roughly opposite in sign to the Klein–Nishina formula.

In summary, it appears that RCS cannot be explained purely perturbatively. It might be explained with the perturbative scattering of a photon and quark, with soft nucleon-structure physics modeled through either quark models or GPDs, but more work needs to be done on improving the energy dependence.

3.2.3. Deeply virtual Compton scattering. VCS is a generalization of RCS, in which a virtual photon emitted by a scattered electron is absorbed by a nucleon, with a real photon emitted—see figure 9. Deep VCS (DVCS) refers to this process at high Q^2. The competing Bethe–Heitler (BH)

[4] Prior to the appearance of the JLab data, it was noted [121] that in the vector meson dominance picture the photon couples through its hadronic component—e.g. the ρ meson—which would naturally lead to an s^{-8} energy dependence. But it was argued that the Cornell data were consistent with s^{-6}, and the VMD contribution was estimated to be perhaps 10% the size of the data.

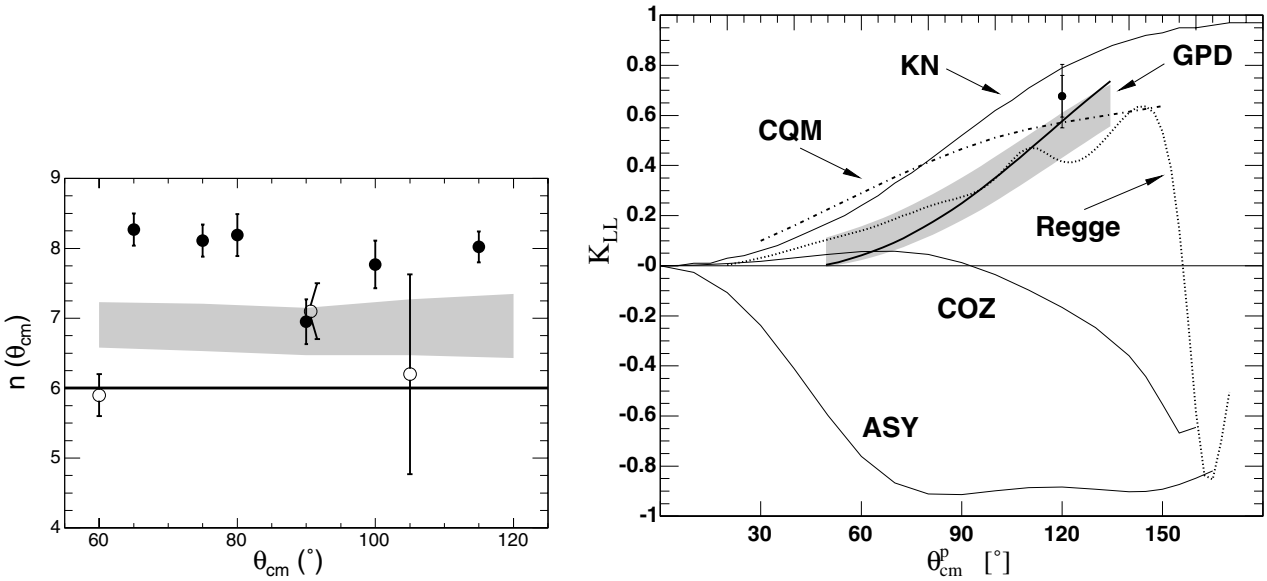

Figure 7. Left: scaling exponent n in $d\sigma/dt(\theta_{cm}) \propto s^{-n}$ as a function of θ_{cm} for RCS. Open circles are from [114], closed circles are from [115] and the gray band represents the scaling exponent predicted by GPD models. The line at $n = 6$ is the expectation from pQCD. Reproduced with permission from [115]. Copyright 2007 American Physical Society. Right: longitudinal polarization transfer coefficient K_{LL}, compared with several calculations. The curve labeled 'KN' is the Klein–Nishina result, for polarization transfer to a point-like spin-1/2 particle. The curves labeled 'ASY' and 'COZ' are pQCD calculations with two different choices for the distribution amplitude. Other calculations include constituent quark ('CQM'), generalized parton distribution ('GPD'), and Regge ('Regge') models. Reproduced with permission from [116]. Copyright 2005 American Physical Society.

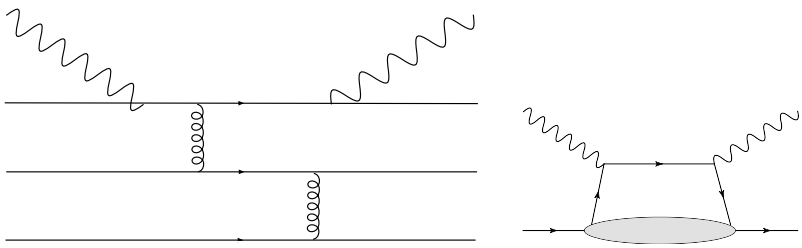

Figure 8. Left: a sample pQCD Feynman diagram for Compton scattering, with the minimal two hard gluon exchanges to share the absorbed photon momentum among the quarks. The absorbed and emitted photons can couple to different quarks. Right: the handbag diagram for RCS, where the absorbed and emitted photons attach to the same quark line, and the momentum is shared with other constituents of the nucleon through the wave function (soft gluon exchanges).

process, in which electrons passing near the nucleus radiate photons, is understood and calculable. Rather than being an annoying background, the BH process is an advantage; similar to the case of holography it can be thought of as providing a reference beam that gives us additional information. The interference of DVCS and BH allows the phase of the DVCS amplitude to be determined. Note that the BH photons are emitted generally in the direction of the emitting electron, and the DVCS process becomes increasingly dominant with increased energy.

Interest in the DVCS process burgeoned with the realization that it could provide important information on GPDs and the total angular momentum of quarks in the nucleon [122] via measurements at large Q^2 and small $-t$. The pQCD diagram and the handbag diagram, which is assumed in the GPD approach, are the same as in figure 8, except that the incoming photon is virtual. While the overwhelming majority of calculations have used the GPD framework, the validity of this approach can be studied to some degree with pQCD calculations. In [117], the DVCS process was calculated and the approximation that the incoming and outgoing photons interact with the same quark was studied. The two photons attaching to the same quark line was dominant for photon scattering angles up to 20°.

A recent review that discusses DVCS data and GPDs is given in [123]. The VCS amplitude in leading order depends on integrals of the GPDs H, $\tilde{H}$, E and $\tilde{E}$ weighted by kinematic factors. The major observables studied have been cross-sections, beam-helicity dependent cross-sections or asymmetries, and longitudinally polarized target asymmetries. The data are generally in the range $Q^2 \approx 1$–$3\,\mathrm{GeV}^2$ and $-t < 1\,\mathrm{GeV}^2$—note that the four-momentum transfer $-t$ is not the same as the photon four-momentum Q^2 as the final state includes $p + \gamma$. Both the neutron and the proton have been studied. At present, the various measurements tend to be qualitatively consistent with GPD models that include some amount of higher order twist-3 contribution, but there is no comprehensive, quantitative explanation.

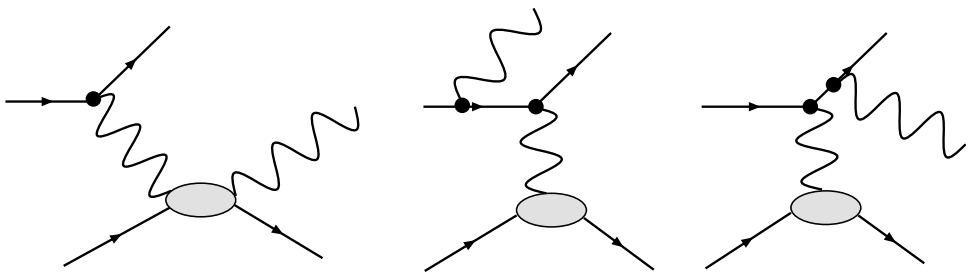

Figure 9. Left: VCS. Middle: the BH process, with a photon emitted by the incoming electron. Right: the BH process, with a photon emitted by the outgoing electron.

3.2.4. Photo–pion reactions. Meson production reactions were among the first pieces of evidence for the constituent count rules [124, 125], yet these reactions have been notoriously difficult to calculate. As pointed out in the pioneering work of [126], pion photoproduction calculations require several thousand Feynman diagrams. The calculated cross-section has a large sensitivity to the baryon wave functions used, is similar in size to the experimental data, and has a potentially interesting helicity structure. However, the numerical techniques used were related to those used in a calculation of Compton scattering [127], which is not in agreement with subsequent work—see [117].

The pQCD calculation is simplified to only hundreds of diagrams in the quark–diquark model of the nucleon [128, 129]. Diquarks may be viewed as effective quasi-elementary particles that incorporate some nonperturbative physics of the nucleon, for reactions in which the interaction is primarily with a single quark. There are spin-0 scalar diquarks and spin-1 diquarks. Photoproduction of $K^+\Lambda^0$ is most studied as it involves only scalar diquarks—the spin of the Λ^0 is usually viewed as being carried by the s quark. The prediction of [129] for the $\gamma p \to \pi^+ n$ reaction is roughly of similar size to the data. A quantitative explanation would require, e.g., additional u-channel processes in the case of the asymptotic distribution amplitude.

More recently there have been GPD based calculations of meson photoproduction [121]. The calculations are about two orders of magnitude below the data. The authors argue that in the GPD picture the formation of a meson likely reduces the cross-section compared with the emission of a photon as in RCS. Since, however, the data show meson production cross-sections are much larger, they suggest other physics must be responsible. The approximate validity of VMD relations between ρ photoproduction and πp scattering, the possible s^{-8} scaling of π^0 photoproduction and the large cross-sections suggest that the VMD picture explains meson photoproduction for several GeV incident photons.

In parallel with these theoretical developments Jefferson Lab experiments have improved our knowledge of meson photoproduction. In [132], recoil proton polarization was measured in the $\gamma p \to \pi^0 p$ reaction for photon energies up to 4 GeV (center-of-mass total energy $W \approx 2.9$ GeV). The polarizations were found to vary with energy and angle, and did not appear to approach any smooth behavior as expected from quark models. A wide range of single pion photoproduction measurements have also now been performed by the CLAS collaboration [130, 133, 134], with a fraction of the data shown in figure 10. It appears that the resonance region extends up to, and the scaling region starts at, $W = \sqrt{s} \approx 2.6$ GeV, much higher than the conventional $W = 2$ GeV limit to the resonance region. In [131, 135], the cross-sections for $\gamma p \to \pi^+ n$ and $\gamma n \to \pi^- p$ were measured to higher W. Figure 10 shows that the ratio of the two processes at the highest energies, but only at $\theta_{cm} = 90^\circ$, agrees with simple quark estimates [121, 136]:

$$\frac{d\sigma(\gamma n \to \pi^- p)}{d\sigma(\gamma p \to \pi^+ n)} \approx \left(\frac{ue_d + se_u}{ue_u + se_d}\right)^2, \tag{8}$$

where s and u are Mandelstam variables and $e_{u,d}$ are the u, d quark charges. Also, the highest energy points in the scaling region appear to have some oscillation about smooth scaling, perhaps of similar origin to the behavior seen in $pp \to pp$ [137]. Thus, there appear to be competing underlying dynamical mechanisms for the pion photoproduction reactions.

3.2.5. Baryon transition form factors. Extracting baryon transition form factors and their asymptotic behavior is difficult, as baryon resonances overlap, are wide, and sit on top of a nonresonant background. Reliable extraction is aided by polarization measurements, by high statistics, by studying multiple decay channels, and by a dynamical model to get at the bare resonance parameters from the observed data, as the final-state hadrons interact. There has been an extensive program at JLab aimed at determining baryon resonance properties—see e.g. [138]. The most studied case, to the highest Q^2, is the $N \to \Delta$ transition; it is the only case we consider here.

The $\Delta(1232)$ resonance, probed at low energies, has long been known to arise from the $L = 1$, $J = 3/2$, $T = 3/2$, or p_{33}, partial wave in πN scattering. In the constituent quark model the nucleon is photo-excited into the Δ resonance primarily by a quark spin flip; with $\Delta J = 1, \Delta L = 0, \Delta S = 1$, this is an $M1$ magnetic dipole transition. There is also a small, few per cent, electric quadrupole, or $E2$, component.

The pQCD result that the proton helicity nonflip Dirac and helicity-flip Pauli form factors fall as Q^{-4} and Q^{-6}, respectively, applies to baryon transition form factors, measured with electroproduction, as well [139]. There are several different common conventions for the three $N \to \Delta$ transition form factors; here we use the magnetic dipole M_{1+}, electric quadrupole E_{1+} and scalar dipole S_{1+}. The asymptotic expectations for these form factors are $R_{EM} \equiv E_{1+}/M_{1+} \to 1$, and $R_{SM} \equiv S_{1+}/M_{1+} \to$ constant, as discussed in [140], with

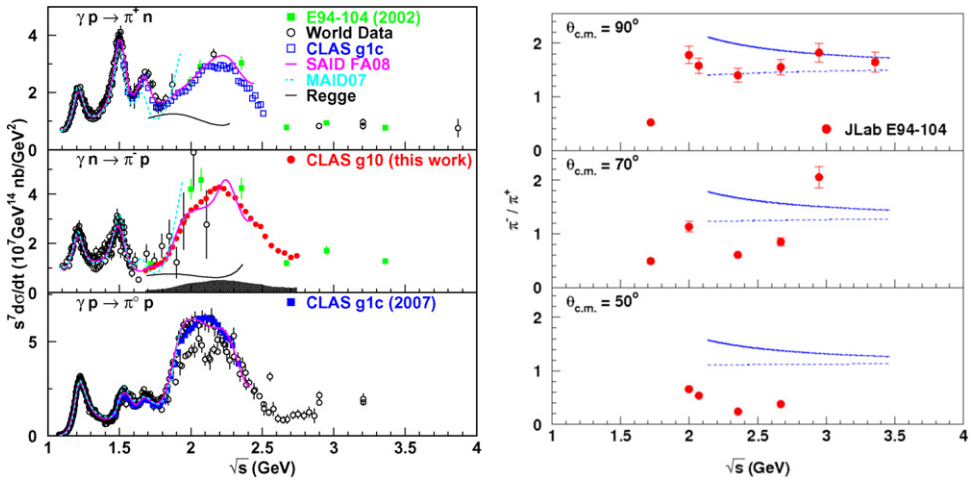

Figure 10. Left: cross-sections for single pion photoproduction at $\theta_{cm} = 90^\circ$ including recent CLAS data. Reproduced with permission from [130]. Copyright 2009 American Physical Society. Right: cross-section ratio $d\sigma(\gamma n \to \pi^- p)/d\sigma(\gamma p \to \pi^+ n)$. Reproduced with permission from [131]. Copyright 2005 American Physical Society. The solid line is from (8), while the dashed line incorporates mass corrections by reducing s and u by m_p^2.

all falling as $1/Q^4$. There is no support for an approach to these limits from data in the measured range $Q^2 = 0 \to 8\,\mathrm{GeV}^2$. The magnetic form factor falls faster than the dipole, which is probably not surprising given the photo-excitation result that R_{EM} is small—there must be a large nonperturbative component to the spin-flip M_{1+} transition. But, in addition, $R_{EM} \approx 2$–3% at all Q^2; the ratio gives no clear indication of increasing toward unity. Finally, R_{SM} gradually drops from about -5% near the real photon point to about -25%—see [138, 141]. Thus, there is no indication of an approach toward the asymptotic predictions.

Nevertheless, several QCD-inspired theoretical approaches—unitary transformation [142], AdS/QCD [143], and QCD sum rules [144]—have been applied reasonably successfully to this transition given the approximations. The unitary transformation approach illustrates the importance of the pion cloud at low Q^2 and the bare nucleon at high Q^2, while the QCD sum rule approach indicates the important cancellations that arise from the valence quark symmetries of the N and the Δ.

4. Color transparency

For decades, it has been speculated that CT will emerge from QCD. In brief, CT occurs when the initial- and final-state interactions become considerably diminished or vanish in hadron–hadron interactions. It is widely believed that three conditions must be met for CT to be observed.

- A hadron must have been formed in a small size state or point-like configuration (PLC).
- Small size hadrons have small cross-sections.
- The small size hadron remains small in size for a significant time during its travel through the nuclear medium.

In particular, searches for the CT effect have been performed for A(p, 2p), A(e, e′p), A(e, e′π) and A(e, e′ρ) reactions as well as pion and J/ψ photoproduction reactions and coherent pion-induced jet production on a nucleus. Thus far, in the A(p, 2p) and A(e, e′p) reactions the evidence [145–149] for CT has not been convincing. There are two possible reasons for this: (i) it is inherently difficult to find or produce a nucleon, a three-quark system, in a small state. A small state for the proton would only occur at extremely high energies where exclusive reactions have little cross-section. (ii) At the relatively low energies of these experiments the expansion of the PLC, if it is indeed produced in the first place, occurs within the nuclear medium.

By contrast, the meson being only an antiquark–quark system offers the possibility that the PLC would be more readily formed than that for a baryon [150, 151]. In fact, evidence has been reported for photoproduction [152, 153] of the pion and J/ψ as well as for electroproduction [154–158] of the pion and ρ meson.

Perhaps the most striking evidence for the CT can be found in coherent nuclear processes where a pion diffracts into two jets of high relative transverse momentum [159]. The experiment was conducted at FNAL where a 500 GeV pion beam was scattered coherently from targets of C and Pt. The results were consistent with the per-nucleus cross-section being $\sigma = \sigma_\circ A^\alpha$. A value of $\alpha = 1.6$ was found which is consistent with predictions [160, 161] of CT. For diffractive processes on single nucleons in the nucleus, the coherent cross-section would grow as A^2, while the elastic form factor would contribute a factor of $A^{-2/3}$. This would lead to an overall prediction of $\alpha = 4/3$. For normal pion inelastic scattering, one should expect $\alpha = 2/3$. Thus, the predicted yield ratio between Pt and C is about an order of magnitude more than expected from ordinary diffraction. This is indeed a strong signal for CT.

A signal for CT is particularly important in indicating when factorization [162–164] occurs in semi-exclusive electro-meson production. In particular, CT in pion electroproduction is a necessary condition for factorization in exclusive electroproduction of pions. Exclusive electroproduction of mesons is believed to be an essential tool

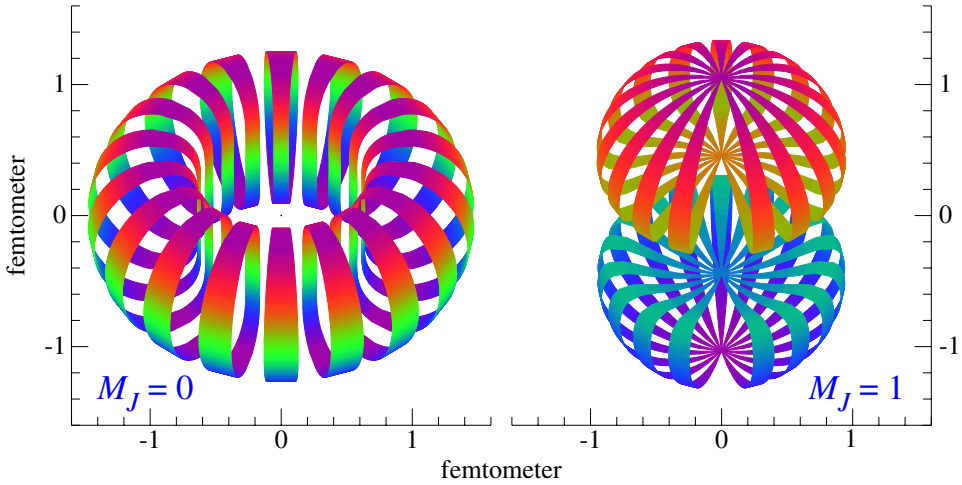

Figure 11. Results of a calculation of the surface at a density of 0.24 nucleons/fm^3 in the deuteron. Adapted from [166].

to access generalized parton distributions at JLab and CERN (COMPASS-II). The most recent search for the onset of CT in meson electroproduction was performed at JLab. In this case, a rho was electroproduced in Fe nuclei. Evidence for a CT effect would be a rise in the transparency of the rho-meson as a function of Q^2. Indeed, evidence for the onset of CT was observed at JLab for the enhancement of transparency of rho mesons at large values of Q^2 [158]. Plans for future experiments at an upgraded JLab are hoped to provide more compelling evidence for the effect in meson electroproduction. It has been suggested [165] that COMPASS-II could also provide information on this effect.

5. The deuteron

5.1. Hadronic descriptions of the deuteron

Gilman and Gross put forward an excellent review [31] of the theoretical and experimental status of studies of the deuteron prior to 2001. Here we present a brief summary of the hadronic description of the deuteron found in this work as well as approaches since 2000. Further, because of the emphasis on the high-momentum transfer in this report, we focus primarily on relativistic calculations of electron–deuteron elastic scattering and two-nucleon photodisintegration of the deuteron after 2000. The deuteron is particularly notable for revealing the role of the tensor force in the nucleon–nucleon interaction. Indeed, the deuteron would not be bound without the tensor force. A particularly good discussion of electron–deuteron elastic scattering that emphasizes the geometric implications of the tensor force on the deuteron structure is given in [166]. In particular, if a deuteron can be aligned in such a fashion that it is in a $M_J = 0$ magnetic substate, where J is the spin of the deuteron, then the deuteron will have a toroidal shape. Whereas, if the deuteron is in a $M_J = 1$ or $M_J = -1$ substate, then it will have a 'dumbbell' shape as shown in figure 11. The hole in the torus is a reflection of the repulsive core of the N–N interaction, while the overall shapes are largely governed by the relatively strong tensor force below 2 fm. If the deuterons are aligned in these magnetic substates, then these shapes strongly influence electron scattering. In this way, electron scattering from aligned deuterons is sensitive to the underlying model of the deuteron, in particular, the influence of the tensor force which gives rise to the deuteron d-state and leads to the non-spherical shapes.

Cross-sections [167–182] and tensor polarizations [183–186] or analyzing powers [187–194] have been measured in electron–deuteron elastic scattering. Since the deuteron has a spin of unity, three form factors—charge, G_E, magnetic, G_M, and quadrupole, G_Q—completely describe these observables. The standard Rosenbluth cross-section for elastic electron scattering is given by

$$\frac{\mathrm{d}\sigma}{\mathrm{d}\Omega} = \sigma_{\mathrm{Mott}}\left[A(Q^2) + B(Q^2)\tan^2(\theta/2)\right], \tag{9}$$

where

$$A = G_C^2 + \frac{2}{3}\eta G_M^2 + \frac{8}{9}\eta^2 G_Q^2, \tag{10}$$

$$B = \frac{4}{3}\eta(1+\eta)G_M^2, \tag{11}$$

and $\eta = Q^2/4M^2$ is a kinematic factor, where M is the deuteron mass. The most informative tensor polarization or analyzing power, T_{20}, often referred to as an alignment, is given by

$$T_{20} = -\frac{\frac{8}{9}\eta^2 G_Q^2 + \frac{8}{3}\eta G_C G_Q + \frac{2}{3}\eta G_M^2\left[\frac{1}{2} + (1+\eta)\tan^2(\theta/2)\right]}{\sqrt{2}\left[A + B\ \tan^2(\theta/2)\right]}. \tag{12}$$

Of course, authors have pointed out that $T_{20} \to -\sqrt{2}$ as $Q^2 \to \infty$ and that this is a sign of the approach to pQCD scaling. However, other estimates, discussed in the next section, indicate a more gradual approach to scaling. World data and two state-of-the-art calculations are shown in figure 12.

Generally, the relativistic treatments of electron–deuteron scattering can be categorized [31] into calculations involving Hamiltonian dynamics and those with propagator dynamics. The former were further categorized into instant form, front form and point form by Dirac [195]. A recent informative review of Poincaré invariant quantum mechanical models is

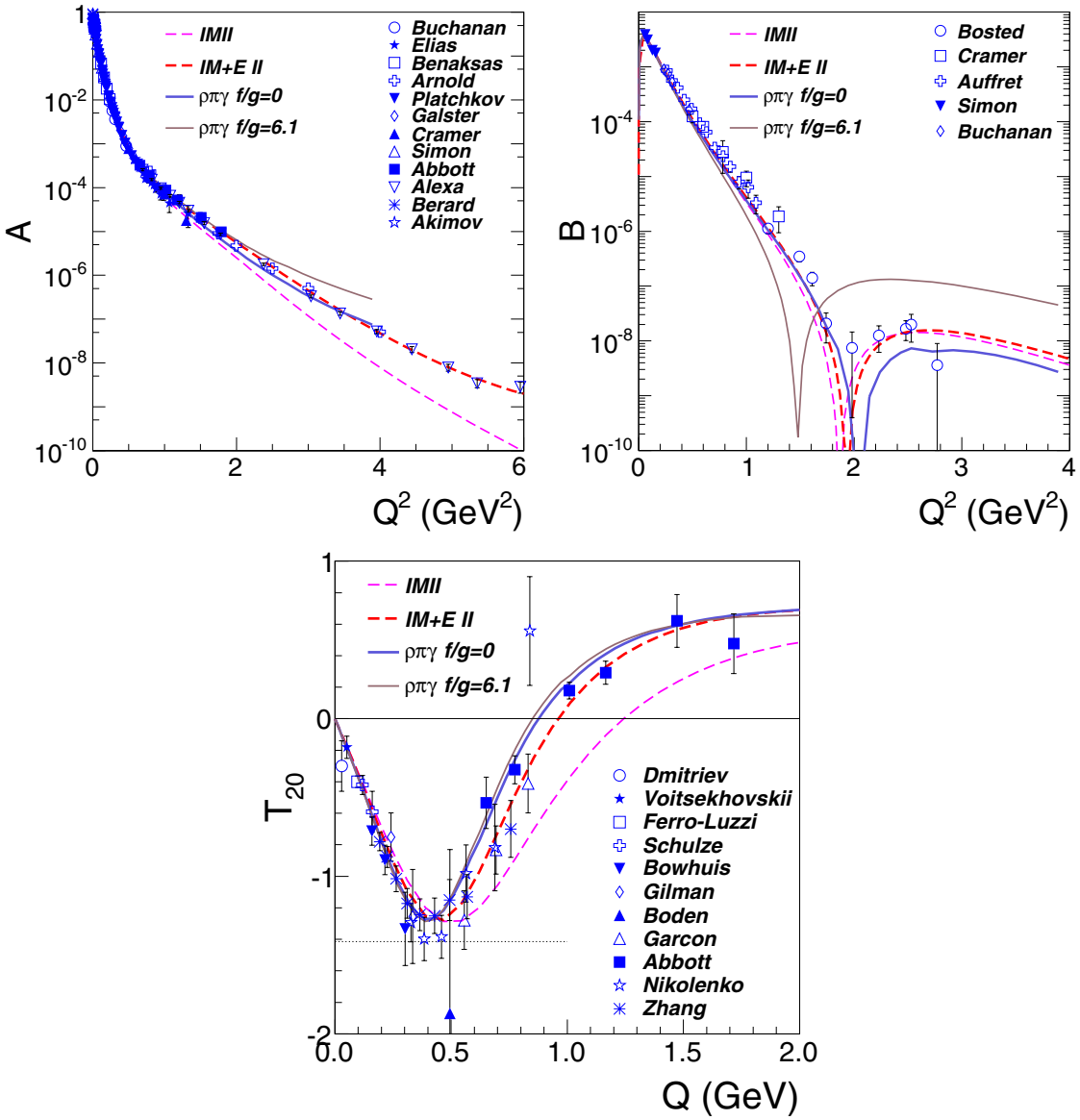

Figure 12. World data for $A(Q^2)$, $B(Q^2)$ and $t_{20} = T_{20}$ in e–d elastic scattering compared with recent meson–nucleon calculations. Shown are a Hamiltonian dynamics calculation [197] without ('IMII') and with ('IM + EII') MEC, and a propagator dynamics calculation [199] ('$\rho\pi\gamma$') with two choices (solid: $f/g = 0$, dash: $f/g = 6.1$) for the tensor strength of the ρNN interaction used in the $\rho\pi\gamma$ exchange current. The best overall description of the data is with the 'IM + EII' calculation.

given in [196]. As pointed out [31], these Hamiltonian-dynamical models suppress negative energy states and lose locality and manifest covariance.

Since 2000 a much better understanding of the nucleon form factors that are necessary for the calculations has become available. For example, the ratio of the electric to magnetic proton form factor, G_{E_p}/G_{M_p}, has changed dramatically compared with pre-2000 nucleon form factor extractions. A recent calculation [197] of electron–deuteron elastic scattering makes use of null plane kinematics in a Poincaré invariant quantum mechanical model and also uses updated nucleon form factors [198] as well as a pair-current-inspired MEC. These calculations [197] of A, B and T_{20} for e–d elastic scattering are shown in figure 12 with curves denoted as IMII (impulse) and IM+EII (impulse+MEC). These results indicate the importance of the MEC in the calculation. Of course, from the discussion in section 2, it is clear that at values of Q^2 currently accessible in the laboratory, the approach to pQCD will not be achieved in e–d elastic scattering. For example, one should expect to approach pQCD near 144 GeV^2. Hence, one should expect the relativistic N–N with MEC approach to provide a reasonable description of the existing data. The MEC have a profound effect on A and B above 1 GeV^2 and on T_{20} above 0.5 GeV^2. It seems likely that MEC would tend to 'mask' any effects from quark–gluon degrees of freedom. Furthermore, because of the small cross-sections, it seems unlikely that the data can be extended to significantly higher values of momentum transfer in the foreseeable future. Nevertheless, B and T_{20} have each been measured by only a single experiment at high Q^2 and new measurements should be performed, perhaps at Mainz or JLab, to confirm our present understanding. While these calculations are in reasonable

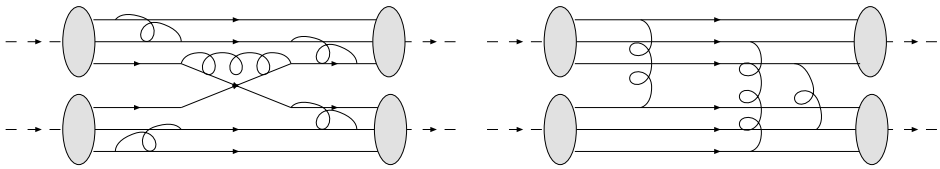

Figure 13. Examples of quark diagrams of NN elastic scattering. Left: elastic scattering by quark interchange, with the momentum transfer shared with other quarks by the exchange of five hard gluons. Right: the independent scattering or Landshoff mechanism, in which each quark of a nucleon exchanges one hard gluon with a different quark of the other nucleon.

agreement with the data, they do not include the $\rho\pi\gamma$ MEC. If this isoscalar MEC were to be included, it is not clear that good agreement could be easily achieved. Further theoretical study is necessary to determine the full effect of this MEC.

The second main approach to relativistic electron–deuteron scattering is the propagator dynamics treatment. Two examples of propagator dynamics are provided by Van Orden *et al* [200] and Phillips *et al* [199]. In the first model, the N–N interaction is described by the exchange of six mesons (π, η, σ, δ, ρ, ω). One of the nucleons is off-shell and has a form factor. This approach is often referred to as the complete impulse approximation (CIA) to distinguish it from the relativistic impulse approximation. The CIA also includes two-body currents. Recent few-body calculations [201] have made use of new high-precision N–N interaction models [202, 203] WJC-1 and WJC-2.

The second example [199] includes relativistic kinematics and the effects of negative energy states. The deuteron is described by the Bonn-B potential, a one-boson exchange model. Here the σ meson coupling was adjusted to give the deuteron binding energy. Boosts of the two-body system and current conservation were imposed on the calculation. In addition, isoscalar MEC were included that involve the $\gamma\pi$ contact term and the $\rho\pi\gamma$ exchange current. Relatively modern nucleon form factors were taken from the work of Kelly [107]. A recent calculation of this type is compared with the data in figure 12.

The results that have a $\rho\pi\gamma$ MEC are in reasonable agreement with the data. However, the value for the tensor strength of the ρNN interaction used in the $\rho\pi\gamma$ exchange current that vanishes gives the best agreement with the data. This value is inconsistent with $f/g = 6.1$ for the Bonn B potential. Nevertheless, it appears possible to explain the data without invoking quark and gluonic degrees of freedom, provided that one takes some freedom with the MEC. A possible future direction may be to consider DSE constraints on MEC processes as indicated in [204].

5.2. Quark–gluon approaches to the N–N interaction and the deuteron

The issue of quark–gluon versus hadronic degrees of freedom was discussed in section 2. In this section we focus on the high-momentum transfer NN interaction, and the high-momentum structure of the deuteron. It is generally accepted for these reactions that only the leading qqq Fock state of the nucleon needs to be considered. As shown in [10], high-energy hadron–hadron reactions which can proceed via quark exchange have cross-sections an order of magnitude larger than reactions which proceed via gluon exchange or quark–antiquark annihilation. This leads to the conclusion that the high-energy NN reaction is dominated by quark-interchange diagrams, such as that shown in figure 13.

The expected scaling for NN elastic scattering is $\mathrm{d}\sigma/\mathrm{d}t \propto s^{-10}$, which is approximately correct in pp $\rightarrow$ pp for $-t > 2.5\,\mathrm{GeV}^2$, $s > 15\,\mathrm{GeV}^2$ [205]. However, the cross-sections oscillate about the s^{-10} scaling [206] and there is also an interesting spin structure [207, 208]. The leading explanations for these observations have been the interference between the pQCD and Landshoff diagrams [209] shown in figure 13, or between the pQCD amplitude and broad heavy quark resonances just above strangeness and charm thresholds [210]. A recent discussion is given in [137]. Thus, while the NN interaction might have an important perturbative quark-exchange component, there clearly are other important contributions.

The quark counting rules lead to the helicity-conserving deuteron form factor scaling as $1/Q^{10}$. The only pQCD calculation of the absolute form factor [211] found a magnitude at least 1000 smaller than existing data, indicating either the dominance of nonperturbative physics or of non-nucleonic, perhaps hidden-color, configurations in the deuteron.

Building on the observations of [10], one can speculate that the deuteron form factor and deuteron photodisintegration reaction are dominated by quark-exchange diagrams such as those shown in figure 14. This is the underlying picture originally adopted for these reactions in the reduced nuclear amplitudes (RNA) approach [212], which works surprisingly well for the helicity-conserving deuteron form factor—here extracted from the A structure function—to quite low Q^2, as shown in figure 15. The reduced form factor $f_D(Q^2)$ was estimated to be a monopole in [212]; the 'BH' line shown uses $(1 + Q^2/m_0^2)^{-1}$ with $m_0 = 0.1\,\mathrm{GeV}$. Subsequently [18] estimated that $f_D(Q^2)$ should vary logarithmically with Q^2 as $(\ln(Q^2/\Lambda^2))^{-1-(2/5)C_F/\beta}/Q^2$; the 'BJL' line shown uses $\Lambda = 0.1\,\mathrm{GeV}$, $C_F = 4/3$ and $\beta = 29/3$. The hard rescattering model discussed further in section 5.3 can be viewed as a further refinement of this approach applied to high-energy photodisintegration, and is the most successful existing explanation of that reaction.

Scaling arguments from pQCD have also been applied to various combinations of the deuteron form factors. Carlson and Gross [213], based on helicity-flips leading to an extra power of Q^2 in the falloff of form factors, estimated that G_M and G_Q fall as Q^{-12} and $G_C/G_Q = 2\eta/3$ where $\eta = Q^2/4M_d^2$. Subsequently, Brodsky and Hiller [214]

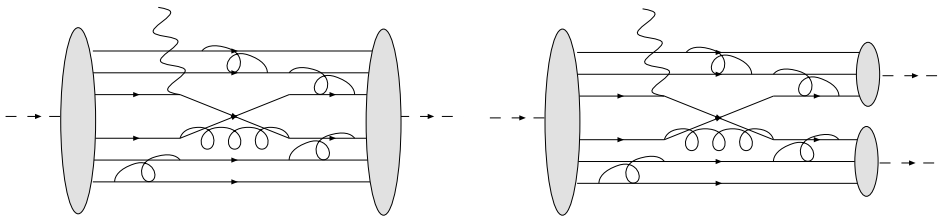

Figure 14. Left: example of a quark-exchange diagram for the deuteron form factor. Right: example of a quark-exchange diagram for deuteron photodisintegration. In each case, the momentum is shared between the struck quark and the other quarks through the exchange of five hard gluons.

found the asymptotic ratio of deuteron form factors to be $G_C : G_M : G_Q = 1 - 2\eta/3 : 2 : -1$. Kobushkin and Syamtomov [215] extended this by including the subleading helicity-flip form factors. The interference between helicity non-flip and helicity-flip form factors allows the fact that B/A is reproduced down to $\approx$1 GeV^2, including the minimum—see figure 15. But the calculation does not reproduce T_{20} well, even though it crosses over the data at $\approx$1 GeV^2 as can also be seen in figure 15. Cao and Wu [216] found the asymptotic ratio of form factors to be $G_C : G_M : G_Q = 1+\frac{8}{3}f+\frac{2}{3}cf^2-\frac{2}{3}\eta : 2(1+f) : -1$. Here f is a parameter determined by the sign change in G_M, c is a constant of order unity and c' is another constant of order unity that does not appear in the asymptotic form factor ratio. This approach leads to results similar to [215]. These issues are reviewed in [217].

The preceding approaches are all based on a perturbative picture of the deuteron. There have also been some efforts at nonpertubative quark models of the NN system. Maltman and Isgur [19] found that the six-quark system strongly clusters into an NN configuration. De Forest and Mulders [218] in a simple model examined the effects of antisymmetrization of quarks in the two nucleons. They concluded that antisymmetrization breaks the concept of factorization, such as that suggested by [212], and becomes increasingly important with increasing momentum. Dijk and Bakker [219] studied the deuteron within the quark-compound bag model. The basic philosophy is that the $A = 2$ system has a short-range six-quark component and a long-range NN component. As shown in [31], the approach yields a good description of deuteron form factors, comparable to the best conventional relativistic NN models. Robson [220] treats the deuteron as a sum of two three-quark harmonic oscillator systems, with quark orbits in the different nucleons required to be orthogonal. The model gives a semi-quantitative description of data; it includes a quark-correlation effect which improves the description, with similar effects to the $\rho\pi\gamma$ meson-exchange term in conventional models. A recent estimate [221] of the effects of 6-, 9-, . . ., quark bags on nuclear structure indicated, for example, that these structures could account for quasi-free electron scattering data at $x > 1$, which are more traditionally interpreted as indications of short-range nucleon correlations in nuclei—see [222] for a discussion of recent experimental results in this area.

In summary, the best approaches to understanding the deuteron structure remain relativistic hadronic models tied to the underlying NN force, despite some uncertainties in this approach. QCD-inspired models have some success. Estimates more firmly based on QCD fail particularly for T_{20}.

5.3. Photodisintegration of the deuteron

The most recent review of deuteron photodisintegration remains [31], where a fuller discussion can be found of physics presented here. The photodisintegration reaction provides large center-of-mass energy W for incident photon energies of a few GeV. In the hadronic picture, hundreds of resonance channels would be potentially excited by E_γ = 4 GeV, which would be natural to sum over in a reaction model with quark–gluon degrees of freedom, just as in deep-inelastic scattering. Also similar to DIS, at GeV energies and large angles there is GeV scale four-momentum transfer $-t$ and $-u$, or equivalently transverse momentum p_T, again suggesting that quark models are appropriate for understanding the reaction dynamics.

Several approaches to the underlying quark dynamics have been developed. A simple pQCD approach [5–7] predicts that cross-sections follow the constituent counting rules, $\mathrm{d}\sigma/\mathrm{d}t \propto s^{-11}$, and polarizations are constrained by hadron helicity conservation, e.g., $p_y = C_{x'} = C_{z'} = 0$. In fact, cross-sections follow the constituent counting rules better than they should, but polarizations do not follow hadron helicity conservation (HHC) [31]. The failure of HHC is no longer surprising. In the DSE approach, massive quarks lead to HHC violating couplings. Furthermore, the importance of quark orbital angular momentum in the structure of the nucleon is now widely appreciated. The RNA approach [212] attempted to extend the validity of the pQCD s dependence to lower energies by including expected threshold kinematic factors, but the simple s^{-11} dependence actually agrees better with the data in the $E_\gamma > 1$ GeV region, as shown in section 6.

The dominance of quark-interchange diagrams in the NN interaction, discussed in section 5.2, leads to the hard rescattering model (HRM). The HRM is based on the photon being absorbed by a pair of quarks being exchanged between the two nucleons, and relates photodisintegration to NN scattering. Because NN data roughly follow the counting rules, photodisintegration should as well. (This general idea was investigated within a different physical model in [223].)

The dominance of planar diagrams in QCD [23] leads to the quark gluon string model (QGS). Deuteron photodisintegration is treated as three-quark exchange, and modeled with nonlinear Regge trajectories, which have been used to describe a number of high-energy reactions, to photodisintegration.

These quark models have provided some insight into the underlying dynamics, along with semi-quantitative predictions

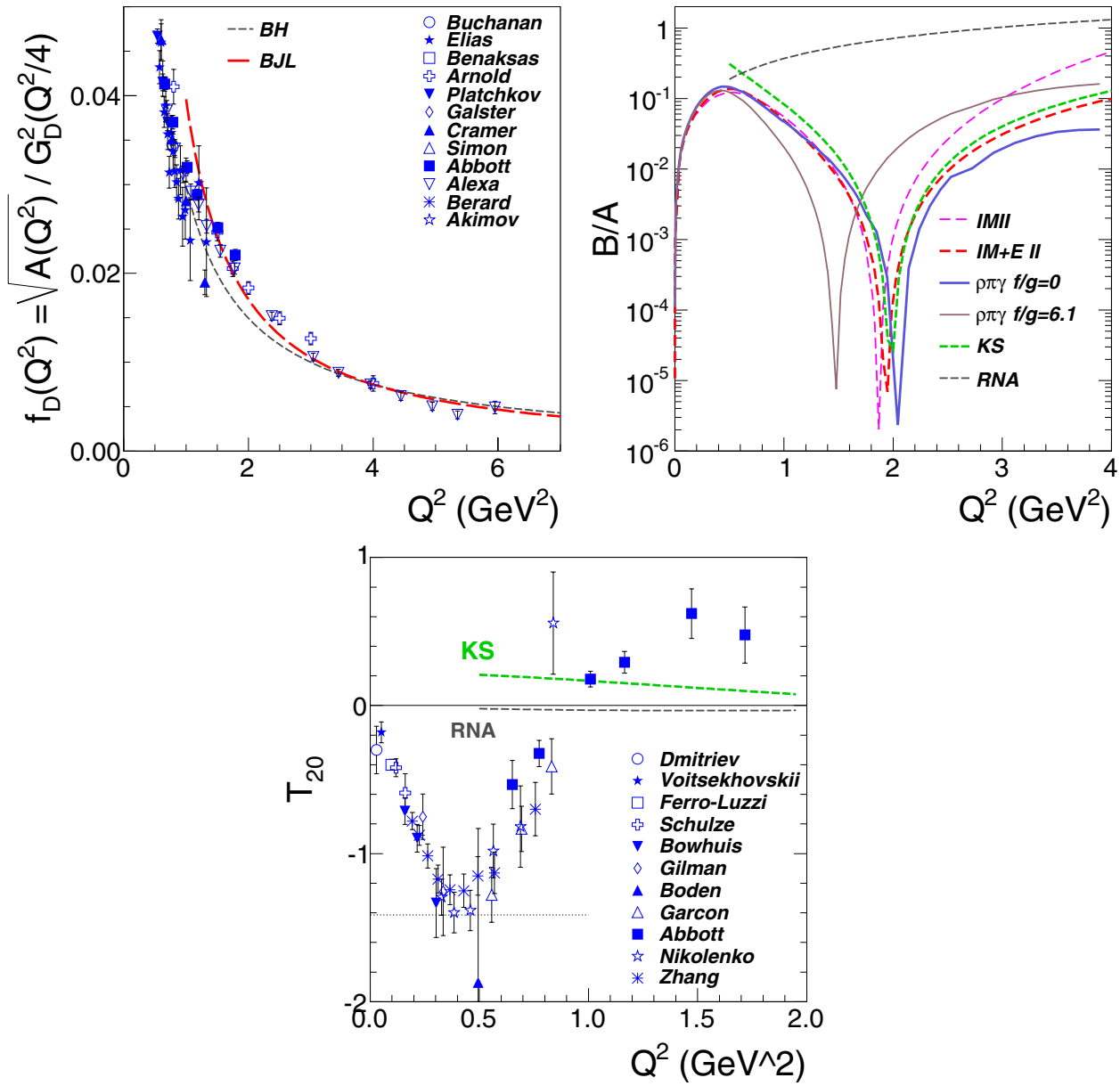

Figure 15. pQCD based estimates for the reduced deuteron form factor $f_d(Q^2)$, the ratio of structure functions B/A, and the polarization T_{20}. For B/A, we compare asymptotic estimates to conventional calculations. The 'RNA' estimate is from [214]. The 'KS' estimate is from [215], using $Q_0^2 = 1.15\,\text{GeV}^2$. The '$\rho\pi\gamma$' calculations use propagator dynamics with different estimates of the $\rho\pi\gamma$ MEC [199]. The 'IMII' and 'IM + EII' conventional calculations use Hamiltonian dynamics [197]. The 'IM + EII' calculation is closest to the data, as shown in figure 12.

of cross-sections and polarizations, but the γd $\rightarrow$ pn data were insufficient at the time of [31] to uniquely identify the underlying dynamics. Since that review, there have been several advances.

Grishina *et al* [224, 225] realized that the pQCD limit for the linearly polarized photon asymmetry, $\Sigma(\theta_{\text{cm}} = 90^\circ) \rightarrow -1$, was due to the assumption of isoscalar photon coupling. For isovector photon coupling, the limit becomes +1. The Σ asymmetry data at 90° are all positive above about 600 MeV, and hint at an increase with energy above 1 GeV.

The CLAS collaboration [226] measured a complete set of angular distributions for E_γ = 0.5–3 GeV and a center-of-mass angle range as much as 10°–160°; these data agree with and dramatically extend earlier angular distribution measurements [227]. The CLAS data demonstrated [228] that the threshold for the scaling behavior is given approximately by $p_T = 1.1\,\text{GeV}/c$, confirming the observation of a p_T threshold, based on a much smaller data set [229].

Tensor polarization asymmetries in deuteron photodisintegration were measured [230] for $E_\gamma \approx$ 70–500 MeV. These data are generally well predicted by modern hadronic theory [231, 232], though detailed differences exist.

An angular distribution of recoil polarizations was measured at $E_\gamma \approx 2$ GeV [233]—see figure 16. The induced polarization and transverse transferred polarization vary with angle so that they cross zero near $\theta_{\text{cm}} = 90^\circ$. In the HRM [234], a natural explanation is that with isovector dominance these polarization components are proportional to the NN

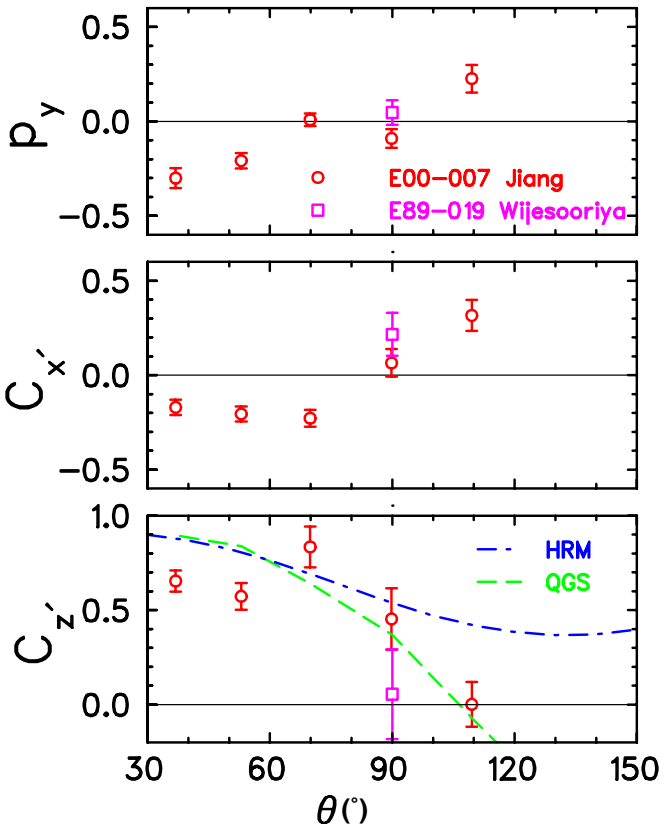

Figure 16. Angular distributions for recoil polarization at $E_\gamma \approx 2$ GeV, adapted from Jiang *et al* [233]. Calculations are from HRM [234] and QGS [224, 225]. The data from E89-019 Wijesooriya *et al* [235] are at $E_\gamma \approx 1.9$ GeV. Adapted from [233].

amplitude ϕ_5 that vanishes at 90°. The longitudinal transferred polarization is large at forward angles and tends to fall with angle. This behavior qualitatively agrees with the predictions shown.

Khokhlov *et al* [236] studied photodisintegration for $E_\gamma = 1.1$–2.3 GeV, using a point-form relativistic quantum mechanics approach with an optical potential derived from NN elastic scattering data up to 3 GeV. Their calculated cross-sections reproduced the data well, but there are no published calculations of polarization observables.

Recoil polarizations were measured for $E_\gamma \approx 280$–360 MeV [237]. This is the region in which the induced proton polarization starts to dramatically diverge from calculations. The behavior was confirmed in a finely binned systematic data set; polarization transfers were also determined. Detailed differences were seen with the best modern hadronic calculations [231, 232].

In summary, while conventional hadronic models provide the best description of low-energy deuteron photodisintegration, it is difficult to extend these models into the GeV region. QCD-inspired models tied to the NN force, the HRM and QGS models, provide both a semi-quantitative description of cross-sections and a qualitative description of some polarization observables. The new high-energy polarization data in particular test models of the underlying dynamics, but the similarity in predictions prevents identifying a correct model. While the focus has now largely turned toward ^{3}He disintegration as a means of understanding the physics, as discussed in section 6, there is interest [238] in testing the recent calculation of [239] of enhanced $\Delta\Delta$ pair production by disintegrating the short-range, six-quark structure of the deuteron.

6. Photoreactions in the light nuclei

Similar to the case for the deuteron, light $A = 3, 4$ nuclei have been studied through elastic scattering. We will not consider the elastic form factors in any detail as, similar to the deuteron case, data can be well explained by conventional nuclear theory with MECs, but do not go to high Q^2. Published elastic ^{3}He and ^{3}H form factor data, e.g., [240, 241], extend only up to ≈ 1.5 GeV^2, while published ^{4}He data [242] are limited to about 2 GeV^2; see [243] for a review. Unpublished data have been taken by the Hall A collaboration up to ≈ 3.5 GeV^2 [244].

High-energy photodisintegration is most studied for ^{3}He. High-energy photodisintegration of ^{3}He leads to pp + $n_{\rm spectator}$, pn + $p_{\rm spectator}$, and three-body final states. The basic idea for the $\gamma\,^3\mathrm{He} \to \mathrm{pp} + n_{\rm spectator}$ reaction [245] is to compare hard pp disintegration from ^{3}He with hard pn disintegration from the deuteron. Models not able to predict the absolute cross-sections might still be able to predict the ratio of these two processes. The initial predictions were for the cross-sections for γpp cross-sections to be similar to or larger than those of γpn; this contrasts with low energies where the γpp cross-sections are an order of magnitude smaller than those for γpn, which is explained by the vanishing magnetic dipole moment for two protons coupled to spin 0. It was also expected in the HRM that due to the observed oscillation in the pp elastic cross-section that γpp cross-section would also exhibit oscillations. The HRM theory was further developed in [246, 247].

The n spectator actually provides some advantages compared with the γd $\to$ pn case. In the impulse approximation, the variation in initial-state neutron momentum varies the γpp center-of-mass energy, so that the energy dependence of the reaction can be measured in a single setting. The neutron light-cone momentum fraction, $\alpha_{\rm n} = (E_{\rm n} - p_{z\rm n})/M$, is nearly unaffected by soft final-state rescatterings, and thus is sensitive to the neutron's wave function—if the γpp disintegration is a short-distance process, this implies large pp momentum in the initial state, which through correlations in the wave function leads to high neutron momentum, and a harder $\alpha_{\rm n}$ distribution. The opposite is true if the γpp process depends on long-range processes.

Figure 17 shows the only published set of high-energy $\gamma\,^3\mathrm{He} \to \mathrm{pp} + \mathrm{n}_{\rm spectator}$ data [255]. The results can be divided into two energy regions. For 1 GeV $< E_\gamma <$ 2 GeV there is a several hundred MeV wide region with a peak or peaks in the $\theta_{\rm cm} = 90°$ cross-sections. At the peak the cross-sections are slightly less than 1/2 of the γpn cross-sections. The origin of this peak is unclear; speculations include three-body processes or resonance excitation—though it should be remembered that there is no indication of resonance excitation in the γd $\to$ pn data in this energy range. For $E_\gamma > 2$ GeV the cross-sections exhibit approximate s^{-11} scaling, at a level a factor of 20 smaller than the γd $\to$ pn data. It is important to

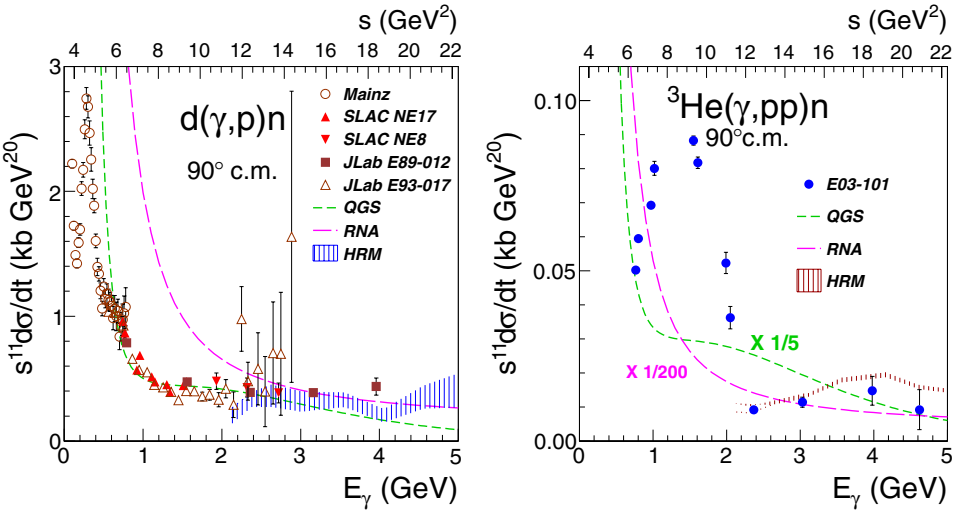

Figure 17. Left: cross-sections for γd $\rightarrow$ pn at $\theta_{cm} = 90^{\circ}$, showing the high-energy s^{-11} scaling. Calculations are labeled QGS [248], RNA [212] and HRM [249]. Data are labeled Mainz [250], NE8 [251, 252], NE17 [253], E89-012 [254] and E93-017 [226]. Right: cross-section for γ^3He $\rightarrow$ pp + $n_{spectator}$, showing the high-energy s^{-11} scaling and the much smaller size of the absolute cross-sections. The RNA and QGS curves have been adjusted by the given factor from their expected magnitudes given in [245] to be of similar size to the data. The HRM calculations are from [246, 247]. The cross-sections shown have an experimental cut $|p_n| < 100$ MeV/c; the estimated correction factor for higher neutron momenta is a factor of two. Adapted from [255].

note that the scaling is indeed the s^{-11} of a two-body process and not the s^{-17} of a three-body process. The idea of a neutron spectator that does not affect the scaling is supported by the data. The small size of the cross-sections was unexpected, and prevented determining the α_n distribution adequately, or whether the fall off is slightly slower than s^{-11} as expected in the HRM. The small size is now understood in the HRM to arise from a cancellation between two NN amplitudes due to opposite signs, which was not recognized in [245]. It is not known at this time whether or not there will be similar effects in the other approaches to the quark dynamics.

Other high-energy photodisintegration experiments include γ^3He $\rightarrow$ ppn, pp+$n_{spectator}$ [256] and γ^4He $\rightarrow$ pt [257], which extend only up to $E_\gamma \approx 1.5$ GeV, not into the scaling region. The γ^3He $\rightarrow$ pd channel has been measured in both JLab Hall A and CLAS, apparently into the scaling region, but is unpublished [258].

7. Perspectives

QCD, proposed more than three decades ago, is the accepted theory of the strong interaction. Nevertheless, the application of QCD to reactions with light nuclei remains elusive. Electromagnetic interactions with hadrons and light nuclei provide the most sensitive test for QCD effects in nuclei since the electromagnetic interaction is relatively well known and calculations can be performed for the simplest systems. Indeed, calculations with perturbative QCD can be performed, however, these calculations have routinely underestimated the exclusive cross-section data at accessible energies. Models involving a factorization process where the incoming high energy photon interacts perturbatively with a quark, but subsequent interactions are relatively soft have had some degree of success. The future theoretical developments likely lie with nonperturbative approaches such as Dyson–Schwinger equations or lattice QCD. It is essential for experiment to map out the long-range behavior of QCD. Future facilities such as the upgraded CEBAF at Jefferson Lab, COMPASS-II at CERN, Drell–Yan experiments at FNAL, J-PARC and RHIC, as well as a possible future electron ion collider hold promise to provide illuminating data for our simplest processes where QCD can be applied.

Although new results for the neutral pion transition form factor from Belle call the puzzling BaBar observations into question, a confirmation of these findings for one of our most elementary processes will be necessary. The form factors for the pion and nucleons will be pushed to significantly higher momentum transfers in the coming decade. These results provide a sensitive determination of the role of dynamical chiral symmetry breaking in the structure of hadrons. While the EMC effect has taught us that the momentum distribution of quarks in bound nucleons is significantly different from those in free nucleons, we do not yet have information on the quark flavor dependence of the EMC effect. The stage is being set to perform new measurements that will reveal this substructure of the EMC effect. The very idea of medium modifications remains controversial, and experimental studies of exclusive reactions probing this area remain inconclusive. While we have had good evidence for a color transparency effect in meson electroproduction, new data from the upgraded CEBAF are necessary to be convincing. While new exclusive photoreaction experiments can be performed at higher energy, the most interesting might be exclusive photopion production since it involves a relatively small number of constituents. The short-range behavior of the deuteron remains a mystery after decades of experimentation and theoretical development. There is only one set of measurements of the magnetic form factor and the tensor polarization in electron–deuteron elastic scattering at high-momentum transfer. The magnetic form factor seems to be best described by calculations with either no

or an incomplete $\rho\pi\gamma$ meson exchange correction. It should be straightforward to provide new measurements of the magnetic form factor in future experiments.

Acknowledgments

The authors especially thank C D Roberts, I C Cloet, D Phillips, S Wallace and W Polyzou for providing tables of their calculations, and D Dutta, M Paolone and I Pomerantz for their help in preparing several of the figures in this work. They also heartily thank K Hafidi, S Pieper, W Polyzou and C D Roberts, for extremely useful discussions. This work was supported by the Department of Energy, Office of Nuclear Physics, contract no DE-AC02-06CH11357 for Argonne National Laboratory and the US National Science Foundation grant PHY 09-69239 for Rutgers University.

References

[1] Bowman P O *et al* 2005 Unquenched quark propagator in Landau gauge *Phys. Rev.* D **71** 054507
[2] Bhagwat M S, Pichowsky M A, Roberts C D and Tandy P C 2003 Analysis of a quenched lattice-QCD dressed-quark propagator *Phys. Rev.* C **68** 015203
[3] Bhagwat M S and Tandy P C 2006 Analysis of full-QCD and quenched-QCD lattice propagators *AIP Conf. Proc.* **842** 225–7
[4] Diakonov D and Petrov V 2000 To what distances do we know the confining potential? *Phys. Scr.* **61** 536–43
[5] Brodsky S J and Farrar G R 1975 Scaling laws for large momentum transfer processes *Phys. Rev.* D **11** 1309
[6] Brodsky S J and Farrar G R 1973 Scaling laws at large transverse momentum *Phys. Rev. Lett.* **31** 1153–6
[7] Matveev V A, Muradyan R M and Tavkhelidze A N 1972 Automodelity in strong interactions *Lett. Nuovo Cimento* **5S2** 907–12
[8] Brodsky S J and Lepage G P 1981 Helicity selection rules and tests of gluon spin in exclusive QCD processes *Phys. Rev.* D **24** 2848
[9] Cosyn W, Martinez M C and Ryckebusch J 2008 Color transparency and short-range correlations in exclusive pion photo- and electroproduction from nuclei *Phys. Rev.* C **77** 034602
[10] White C G *et al* 1994 Comparison of 20 exclusive reactions at large *t* *Phys. Rev.* D **49** 58–78
[11] Roberts C D 2008 Hadron properties and Dyson–Schwinger equations *Prog. Part. Nucl. Phys.* **61** 50–65
[12] Bloom E D and Gilman F J 1970 Scaling, duality, and the behavior of resonances in inelastic electron–proton scattering *Phys. Rev. Lett.* **25** 1140
[13] Melnitchouk W, Ent R and Keppel C 2005 Quark–hadron duality in electron scattering *Phys. Rep.* **406** 127–301
[14] Asaturyan R *et al* 2012 Semi-inclusive charged-pion electroproduction off protons and deuterons: cross sections, ratios and access to the quark–parton model at low energies *Phys. Rev.* C **85** 015202
[15] Isgur N 2000 Feynman brainwashed? *Phys. Today* **53** (8) 11 Letter
[16] Harvey M 1981 On the fractional-parentage expansions of color-singlet six-quark states in a cluster model *Nucl. Phys.* A **352** 301–25
[17] Harvey M 1981 Effective nuclear forces in the quark model with delta and hidden-color channel coupling *Nucl. Phys.* A **352** 326–42
[18] Brodsky S J, Ji C-R and Lepage G P 1983 Quantum chromodynamic predictions for the deuteron form-factor *Phys. Rev. Lett.* **51** 83
[19] Maltman K and Isgur N 1984 Nuclear physics and the quark model: six quarks with chromodynamics *Phys. Rev.* D **29** 952–77
[20] Guichon P A M and Thomas A W 2004 Quark structure and nuclear effective forces *Phys. Rev. Lett.* **93** 132502
[21] Ralston J P 2008 Exploring confinement with spin arXiv:0810.0871v1[hep-ph]
[22] Skyrme T H R 1961 A nonlinear field theory *Proc. R. Soc. Lond.* A **260** 127–38
[23] 't Hooft G 1974 A two-dimensional model for mesons *Nucl. Phys.* B **75** 461
[24] Eisenberg J M and Kaelbermann G 1996 The nucleon–nucleon force from skyrmions *Prog. Part. Nucl. Phys.* **36** 321–34
[25] Nyman E M and Riska D O 1990 Low-energy properties of baryons in the Skyrme model *Rep. Prog. Phys.* **53** 1137
[26] Acus A, Norvaišas E and Riska D O 2006 The α particle as a canonically quantized multiskyrmion *Phys. Rev.* C **74** 025203
[27] Park B-Y, Kim J-I and Rho M 2010 Kaons in dense half-skyrmion matter *Phys. Rev.* C **81** 035203
[28] Weinberg S 1990 Nuclear forces from chiral lagrangians *Phys. Lett.* B **251** 288–92
[29] Epelbaum E, Hammer H-W and Meißner U-G 2009 Modern theory of nuclear forces *Rev. Mod. Phys.* **81** 1773–825
[30] Beane S R, Bedaque P F, Savage M J and van Kolck U 2002 Towards a perturbative theory of nuclear forces *Nucl. Phys.* A **700** 377–402
[31] Gilman R and Gross F 2002 Electromagnetic structure of the deuteron *J. Phys. G: Nucl. Part. Phys.* **28** R37–R116
[32] Phillips D R, Rupak G and Savage M J 2000 Improving the convergence of nn effective field theory *Phys. Lett.* B **473** 209–18
[33] Phillips D R 2007 Chiral effective theory predictions for deuteron form factor ratios at low Q^2. *J. Phys. G: Nucl. Part. Phys.* **34** 365
[34] Walzl M and Meissner U G 2001 Elastic electron deuteron scattering in chiral effective field theory *Phys. Lett.* B **513** 37–45
[35] Benhar O, Day D and Sick I 2008 Inclusive quasi-elastic electron–nucleus scattering *Rev. Mod. Phys.* **80** 189–224
[36] Wallace S J and Tjon J A 2008 Coulomb corrections in quasi-elastic scattering: tests of the effective-momentum approximation *Phys. Rev.* C **78** 044604
[37] Meziani Z-E *et al* 2005 Jefferson Lab experiment E05-110
[38] Paolone M *et al* 2010 Polarization transfer in the ^{4}He(e, e′p)^{3}H Reaction at $Q^2 = 0.8$ and 1.3 (GeV/c)^2 *Phys. Rev. Lett.* **105** 072001
[39] Dieterich S *et al* 2001 Polarization transfer in the $^4\mathrm{He}(\vec{\mathrm{e}}, \mathrm{e}'\vec{\mathrm{p}})^3\mathrm{H}$ reaction *Phys. Lett.* B **500** 47–52
[40] Strauch S *et al* 2003 Polarization transfer in the $^4\mathrm{He}(\vec{\mathrm{e}}, \mathrm{e}'\vec{\mathrm{p}})^3\mathrm{H}$ reaction up to $Q^2 = 2.6$-(GeV/c)^2 *Phys. Rev. Lett.* **91** 052301
[41] Udias J M, Caballero J A, Moya de Guerra E, Jose Enrique Amaro and Donnelly T W 1999 Quaiselastic scattering from relativistic bound nucleons: transverse-longitudinal response *Phys. Rev. Lett.* **83** 5451–4
[42] Lu D-H, Thomas A W, Tsushima K, Williams A G and Saito K 1998 In-medium electron nucleon scattering *Phys. Lett.* B **417** 217–23
[43] Smith J R and Miller G A 2004 Chiral solitons in nuclei: electromagnetic form factors *Phys. Rev.* C **70** 065205
[44] Ciofi degli Atti C, Frankfurt L L, Kaptari L P and Strikman M I 2007 On the dependence of the wave function of a bound nucleon on its momentum and the EMC effect *Phys. Rev.* C **76** 055206

[45] Schiavilla R, Benhar O, Kievsky A, Marcucci L E and Viviani M 2005 Polarization transfer in ^{4}He($\vec{e}$, e′$\vec{p}$)^{3}H is the ratio $G(E(p))/G(M(p))$ modified in medium? *Phys. Rev. Lett.* **94** 072303

[46] Cloet I C, Miller G A, Piasetzky E and Ron G 2009 Neutron properties in the medium *Phys. Rev. Lett.* **103** 082301

[47] Aubert J J *et al* 1983 The ratio of the nucleon structure functions f_2 (n) for iron and deuterium *Phys. Lett.* B **123** 275

[48] Miller G A and Smith J R 2001 Return of the EMC effect *Phys. Rev.* C **65** 015211

[49] Benhar O, Pandharipande V R and Sick I 1997 Nuclear binding and deep inelastic scattering *Phys. Lett.* B **410** 79–85

[50] Benhar O, Pandharipande V R and Sick I 2000 Many body theory interpretation of deep inelastic scattering *Phys. Lett.* B **489** 131–6

[51] Frankfurt L and Strikman M 2010 Photon parton distributions in nuclei and the EMC effect *Phys. Rev.* C **82** 065203

[52] Seely J *et al* 2009 New measurements of the EMC effect in very light nuclei *Phys. Rev. Lett.* **103** 202301

[53] Weinstein L B *et al* 2011 Short range correlations and the EMC effect *Phys. Rev. Lett.* **106** 052301

[54] Isenhower L D *et al* 2001 Proposal for Drell–Yan measurements of nucleon and nuclear structure with the FNAL main injector Spokespeople: D F Geesaman and P E Reimer, http://www.phy.anl.gov/mep/SeaQuest/

[55] Petratos G G *et al* 2006 Jefferson Lab experiment E12-06-118.

[56] Cloët I C, Bentz W and Thomas A W 2005 Spin-dependent structure functions in nuclear matter and the polarized EMC effect *Phys. Rev. Lett.* **95** 052302

[57] Lepage G P and Brodsky S J 1979 Exclusive processes in quantum chromodynamics: evolution equations for hadronic wave functions and the form-factors of mesons *Phys. Lett.* B **87** 359–65

[58] Farrar G R and Jackson D R 1979 The pion form-factor *Phys. Rev. Lett.* **43** 246

[59] Gutierrez-Guerrero L X, Bashir A, Cloet I C and Roberts C D 2010 Pion form factor from a contact interaction *Phys. Rev.* C **81** 065202

[60] Bjorken J D 1967 *Proc. 3rd Int. Conf. on Electron and Photon Interactions (Clearing House of Federal Scientific and Technical Information, Washington, DC.)*

[61] Bjorken J D and Paschos E A 1969 Inelastic electron proton and gamma proton scattering, and the structure of the nucleon *Phys. Rev.* **185** 1975–82

[62] Feynman R P 1969 Very high-energy collisions of hadrons *Phys. Rev. Lett.* **23** 1415–7

[63] Amendolia S R *et al* 1986 A measurement of the space-like pion electromagnetic form-factor *Nucl. Phys.* B **277** 168

[64] Dally E B *et al* 1981 Measurement of the pion form factor *Phys. Rev.* D **24** 1718–35

[65] Dally E B *et al* 1982 Elastic scattering measurement of the negative pion radius *Phys. Rev. Lett.* **48** 375–8

[66] Tadevosyan V *et al* 2007 Determination of the pion charge form factor for $Q^2 = 0.60$–$1.60\,\mathrm{GeV}^2$ *Phys. Rev.* C **75** 055205

[67] Blok H P *et al* 2008 Charged pion form factor between $Q^2 = 0.60$ and $2.45\,\mathrm{GeV}^2$: I. Measurements of the cross section for the ^{1}H(e, e′π^+)n reaction *Phys. Rev.* C **78** 045202

[68] Huber G M *et al* 2008 Charged pion form factor between $Q^2 = 0.60$ and $2.45\,\mathrm{GeV}^2$: II. Determination of, and results for, the pion form factor *Phys. Rev.* C **78** 045203

[69] Barkov L M *et al* 1985 Electromagnetic pion form-factor in the timelike region *Nucl. Phys.* B **256** 365–84

[70] Grigoryan H R and Radyushkin A V 2007 Pion form factor in chiral limit of hard-wall AdS/QCD model *Phys. Rev.* D **76** 115007

[71] Cloet I C and Roberts C D 2008 Form factors and Dyson–Schwinger equations *Proc. Sci.* **LC2008** 047

[72] Brommel D *et al* 2007 The pion form factor from lattice QCD with two dynamical flavours *Eur. Phys. J.* C **51** 335–45

[73] de Teramond G F and Brodsky S J 2009 Light-front holography: a first approximation to QCD *Phys. Rev. Lett.* **102** 081601

[74] Bakulev A P, Passek-Kumericki K, Schroers W and Stefanis N G 2004 Pion form factor in QCD: from nonlocal condensates to NLO analytic perturbation theory *Phys. Rev.* D **70** 033014

[75] Volmer J *et al* 2001 New results for the charged pion electromagnetic form-factor *Phys. Rev. Lett.* **86** 1713–16

[76] Milana J, Nussinov S and Olsson M G 1993 Does $J/\psi \to \pi^+\pi^-$ fix the electromagnetic form- factor $F_\pi(t)$ at $t = M2^2_{J/\psi}$? *Phys. Rev. Lett.* **71** 2533–6

[77] Seth K K 2008 Timelike formfactors of pion, kaon, and proton at large momentum transfers *Proc. Sci.* **8** 081 (Confinement)

[78] Lepage P G and Brodsky S J 1980 Exclusive processes in perturbative quantum chromodynamics *Phys. Rev.* D **22** 2157

[79] Aubert B *et al* 2009 Measurement of the $\gamma\gamma* \longrightarrow \pi^\circ$ transition form factor *Phys. Rev.* D **80** 052002

[80] Dubrovin M 2010 Measurement of the $\gamma\gamma* \longrightarrow \pi^\circ$ transition form factor *Proc. Sci.* **LC2010** 060

[81] Dorokhov A E 2010 Photon-pion transition form factor at high photon virtualities within the nonlocal chiral quark model *JETP Lett.* **92** 707–19

[82] Dorokhov A 2010 Photon-pion transition form factor within nonlocal chiral quark model *Proc. Sci.* **LC2010** 061

[83] Gorchtein M, Guo P and Szczepaniak A P 2011 Pion form factors arXiv:1102.5558[nucl-th]

[84] Pham T N and Pham X Y 2011 Chiral anomaly, triangle loop and the the $\gamma\gamma^* \to \pi^0$ form factor arXiv:1103.0452[hep-th]

[85] Roberts H L L, Roberts C D, Bashir A, Gutierrez-Guerrero L X and Tandy P C 2010 Abelian anomaly and neutral pion production *Phys.Rev.* C **82** 065202

[86] Chang L, Roberts C D and Tandy P C 2011 Selected highlights from the study of mesons arXiv:1107.4003v2[nucl-th]

[87] Mikhailov S V and Stefanis N G 2009 Pion transition form factor at the two-loop level vis-a-vis experimental data *Mod. Phys. Lett.* A **24** 2858–67

[88] Brodsky S J, Cao F-G and de Teramond G F 2011 Evolved QCD predictions for the meson-photon transition form factors *Phys. Rev.* D **84** 033001

[89] Bakulev A P, Mikhailov S V, Pimikov A V and Stefanis N G 2011 Pion-photon transition: the new QCD frontier *Phys. Rev.* D **84** 034014

[90] Brodsky S J, Cao F-G and de Teramond G F 2011 Meson transition form factors in light-front holographic QCD *Phys. Rev.* D **84** 075012

[91] del Amo Sanchez P *et al* 2011 Measurement of the $\gamma\gamma^* \to \eta$ and $\gamma\gamma^* \to \eta'$ transition form factors *Phys. Rev.* D **84** 052001

[92] Lees J P *et al* 2010 Measurement of the $\gamma\gamma^* \longrightarrow \eta_c$ transition form factor *Phys. Rev.* D **81** 052010

[93] Uehara S *et al* 2012 Measurement of $\gamma\gamma^* \to \pi^0$ transition form factor at Belle arXiv:1205.3249v1 [hep-ex]

[94] Arrington J, Roberts C D and Zanotti J M 2007 Nucleon electromagnetic form-factors *J. Phys. G: Nucl. Part. Phys.* **34** S23–51

[95] Arnold R G *et al* 1986 Measurement of elastic electron scattering from the proton at high momentum transfer *Phys. Rev. Lett.* **57** 174

[96] Lachniet J *et al* 2009 A precise measurement of the neutron magnetic form factor G_M^n in the few GeV^2 region *Phys. Rev. Lett.* **102** 192001

[97] Puckett A J R *et al* 2010 Recoil polarization measurements of the proton electromagnetic form factor ratio to $Q^2 = 8.5\,GeV^2$ *Phys. Rev. Lett.* **104** 242301

[98] Riordan S *et al* 2010 Measurements of the electric form factor of the neutron up to $Q^2 = 3.4\,GeV^2$ using the reaction ^{3}He(e, e′n)pp *Phys. Rev. Lett.* **105** 262302

[99] Isgur N and Llewellyn Smith C H 1984 Asymptopia in high q^2 exclusive processes in QCD *Phys. Rev. Lett.* **52** 1080

[100] Jones M K *et al* 2000 G_{E_p}/G_{M_p} ratio by polarization transfer in $\vec{e}p \to e\vec{p}$ *Phys. Rev. Lett.* **84** 1398–402

[101] Miller G A and Frank M R 2002 Q^2 independence of QF_2/F_1, Poincaré invariance and the non-conservation of helicity *Phys. Rev.* C **65** 065205

[102] Belitsky A V, Ji X-d and Yuan F 2003 A perturbative QCD analysis of the nucleon's Pauli form factor $F_2(Q^2)$ *Phys. Rev. Lett.* **91** 092003

[103] Brodsky S J, Hiller J R, Hwang D S and Karmanov V A 2004 Covariant structure of light-front wave functions and the behavior of hadronic form factors *Phys. Rev.* D **69** 076001

[104] Cloet I C, Eichmann G, El-Bennich B, Klahn T and Roberts C D 2009 Survey of nucleon electromagnetic form factors *Few Body Syst.* **46** 1–36

[105] Chang L, Liu Y-X and Roberts C D 2011 Dressed-quark anomalous magnetic moments *Phys. Rev. Lett.* **106** 072001

[106] Chang L, Cloet I C, Roberts C D and Roberts H L L 2011 T(r)opical Dyson–Schwinger equations *AIP Conf. Proc.* **1354** 110–17

[107] Kelly J J 2004 Simple parametrization of nucleon form factors *Phys. Rev.* C **70** 068202

[108] Arrington J, Melnitchouk W and Tjon J A 2007 Global analysis of proton elastic form factor data with two-photon exchange corrections *Phys. Rev.* C **76** 035205

[109] Punjabi V *et al* 2005 Proton elastic form-factor ratios to $Q^2 = 3.5\,GeV^2$ by polarization transfer *Phys.Rev.* C **71** 055202

[110] Gayou O *et al* 2002 Measurement of $G(E_p)/G(M_p)$ in polarized-ep → e polarized-p to $Q^2 = 5.6\,GeV^2$ *Phys. Rev. Lett.* **88** 092301

[111] Glazier D I *et al* 2005 Measurement of the electric form-factor of the neutron at $Q^2 = 0.3$-$(GeV/c)^2$ to 0.8-$(GeV/c)^2$ *Eur. Phys. J.* A **24** 101–9

[112] Plaster B *et al* 2006 Measurements of the neutron electric to magnetic form-factor ratio $G(E_n)/G(M_n)$ via the H-2(polarized-e, e-prime,polarized-n)H-1 reaction to $Q^2 = 1.45$-$(GeV/c)^2$ *Phys. Rev.* C **73** 025205

[113] Warren G *et al* 2004 Measurement of the electric form-factor of the neutron at $Q^2 = 0.5\,GeV^2/c^2$ and $1.0\,GeV^2/c^2$ *Phys. Rev. Lett.* **92** 042301

[114] Shupe M A *et al* 1979 Neutral pion photoproduction and proton Compton scattering at large angles *Phys. Rev.* D **19** 1921–30

[115] Danagoulian A *et al* 2007 Compton scattering cross section on the proton at high momentum transfer *Phys. Rev. Lett.* **98** 152001

[116] Hamilton D J *et al* 2005 Polarization transfer in proton Compton scattering at high momentum transfer *Phys. Rev. Lett.* **94** 242001

[117] Thomson R, Pang A and Ji C-R 2006 Real and virtual nucleon Compton scattering in the perturbative limit *Phys. Rev.* D **73** 054023

[118] Miller G A 2004 Handling the handbag diagram in Compton scattering on the proton *Phys. Rev.* C **69** 052201

[119] Huang H W, Kroll P and Morii T 2002 Perturbative and non-perturbative QCD corrections to wide-angle Compton scattering *Eur. Phys. J.* C **23** 301–10

[120] Kroll P 2007 Wide-angle exclusive scattering: an update *Nucl. Phys.* A **782** 77–85

[121] Huang H W and Kroll P 2000 Large momentum transfer electroproduction of mesons *Eur. Phys. J.* C **17** 423–35

[122] Ji X-D 1997 Gauge invariant decomposition of nucleon spin *Phys. Rev. Lett.* **78** 610–13

[123] Hyde C E, Guidal M and Radyushkin A V 2011 Deeply virtual exclusive processes and generalized parton distributions *J. Phys. Conf. Ser.* **299** 012006

[124] Anderson R L *et al* 1976 Measurements of exclusive photoproduction processes at large values of t and u from 4 GeV to 7.5 GeV *Phys. Rev.* D **14** 679

[125] Clifft R W, Dainton J B, Gabathuler E, Littenberg L S, Marshall R, Rock S E, Thompson J C, Ward D L and Brookes G R 1977 Observation of a baryon exchange dip and parton effects in backward photoproduction of ω *Phys. Lett.* B **72** 144–8

[126] Farrar G R, Huleihel K and Zhang H-Y 1991 Perturbative QCD predictions for large momentum transfer photoproduction *Nucl. Phys.* B **349** 655–74

[127] Farrar G R and Zhang H-y 1990 Perturbative QCD calculation of real and virtual Compton scattering *Phys. Rev.* D **41** 3348

[128] Kroll P 1996 Diquark model predictions for photon induced exclusive reactions arXiv:9607277vI

[129] Folberth G, Rossmann R and Schweiger W 1996 Exclusive photo- and electroproduction of mesons in the GeV region arXiv:hep-ph/9702328vI

[130] Chen W *et al* 2009 A Measurement of the differential cross section for the reaction $\gamma n \to \pi^- p$ from deuterium *Phys. Rev. Lett.* **103** 012301

[131] Zhu L Y *et al* 2005 Cross section measurements of charged pion photoproduction in hydrogen and deuterium from 1.1 GeV to 5.5 GeV *Phys. Rev.* C **71** 044603

[132] Wijesooriya K *et al* 2002 Polarization measurements in neutral pion photoproduction *Phys. Rev.* C **66** 034614

[133] Dugger M *et al* 2007 π^0 photoproduction on the proton for photon energies from 0.675 to 2.875 GeV *Phys. Rev.* C **76** 025211

[134] Dugger M *et al* 2009 π^+ photoproduction on the proton for photon energies from 0.725 to 2.875 GeV *Phys. Rev.* C **79** 065206

[135] Zhu L Y *et al* 2003 Cross section measurement of charged pion photoproduction from hydrogen and deuterium *Phys. Rev. Lett.* **91** 022003

[136] Afanasev A, Carlson C E and Wahlquist C 1997 Probing polarized parton distributions with meson photoproduction *Phys. Lett.* B **398** 393–9

[137] Dutta D and Gao H 2005 The generalized counting rule and oscillatory scaling *Phys. Rev.* C **71** 032201

[138] Aznauryan I, Burkert V D, Lee T-S H and Mokeev V I 2011 Results from the N* program at JLab *J. Phys. Conf. Ser.* **299** 012008

[139] Peter Lepage G and Brodsky S J 1979 Exclusive processes in quantum chromodynamics: the form-factors of baryons at large momentum transfer *Phys. Rev. Lett.* **43** 545–9

[140] Drechsel D and Walcher T 2008 Hadron structure at low q^2 *Rev. Mod. Phys.* **80** 731–85

[141] Gilman R, Holt R J and Stoler P 2011 Transition to perturbative QCD *J. Phys. Conf. Ser.* **299** 012009

[142] Sato T and Lee T-S H 2009 Dynamical models of the excitations of nucleon resonances *J. Phys. G: Nucl. Part. Phys.* **36** 073001

[143] Grigoryan H R, Lee T-S H and Yee H-U 2009 Electromagnetic nucleon-to-delta transition in holographic QCD *Phys. Rev.* D **80** 055006

[144] Carlson C E and Poor J L 1988 Distribution amplitudes and electroproduction of the Δ and other low lying resonances *Phys. Rev.* D **38** 2758

[145] Mardor I *et al* 1998 Nuclear transparency in large momentum transfer quasielastic scattering *Phys. Rev. Lett.* **81** 5085–8

[146] Aclander J L S *et al* 2004 Nuclear transparency in 90-degrees-cm quasielastic A(p, 2p) reactions *Phys. Rev.* C **70** 015208

[147] Makins N *et al* 1994 Momentum transfer dependence of nuclear transparency from the quasielastic ^{12}C(e, e′p) reaction *Phys. Rev. Lett.* **72** 1986–9

[148] Garrow K *et al* 2002 Nuclear transparency from quasielastic A(e, e′p) reactions up to $Q^2 = 8.1$-(GeV/c)^2 *Phys. Rev.* C **66** 044613

[149] Rohe D *et al* 2005 Nuclear transparency from quasielastic ^{12}C(e, e′p) *Phys. Rev.* C **72** 054602

[150] Heiselberg H, Baym G, Blaettel B, Frankfurt L L and Strikman M 1991 Color transparency, color opacity, and fluctuations in nuclear collisions *Phys. Rev. Lett.* **67** 2946–9

[151] Baym G 1996 Color transparency and cross-section fluctuations in hadronic collisions *Adv. Nucl. Phys.* **22** 101–21

[152] Dutta D *et al* 2003 Nuclear transparency with the γn $\longrightarrow \pi^-$p process in He-4 *Phys. Rev.* C **68** 021001

[153] Sokoloff M D *et al* 1986 An experimental study of the A-dependence of J/ψ photoproduction *Phys. Rev. Lett.* **57** 3003

[154] Airapetian A *et al* 2003 The Q^2-dependence of nuclear transparency for exclusive ρ° production *Phys. Rev. Lett.* **90** 052501

[155] Clasie B *et al* 2007 Measurement of nuclear transparency for the A(e, e′π^+) reaction *Phys. Rev. Lett.* **99** 242502

[156] Qian X *et al* 2010 Experimental tudy of the A(e, e′π^+) Reaction on ^{1}H, ^{2}H, ^{12}C, ^{27}Al, ^{63}Cu and ^{197}Au *Phys. Rev.* C **81** 055209

[157] Adams M R *et al* 1995 Measurement of nuclear transparencies from exclusive ρ^0 meson production in muon–nucleus scattering at 470 GeV *Phys. Rev. Lett.* **74** 1525–9

[158] El Fassi L *et al* 2012 Evidence for the onset of color transparency in ρ^0 electroproduction off nuclei *Phys. Lett.* B **712** 326–30

[159] Aitala E M *et al* 2001 Observation of color-transparency in diffractive dissociation of pions *Phys. Rev. Lett.* **86** 4773–7

[160] Bertsch G, Brodsky S J, Goldhaber A S and Gunion J F 1981 Diffractive excitation in QCD *Phys. Rev. Lett.* **47** 297

[161] Frankfurt L, Miller G A and Strikman M 1993 Coherent nuclear diffractive production of mini-jets: illuminating color transparency *Phys. Lett.* B **304** 1–7

[162] Brodsky S J, Frankfurt L, Gunion J F, Mueller A H and Strikman M 1994 Diffractive leptoproduction of vector mesons in QCD *Phys. Rev.* D **50** 3134–44

[163] Collins J C, Frankfurt L and Strikman M 1997 Factorization for hard exclusive electroproduction of mesons in QCD *Phys. Rev.* D **56** 2982–3006

[164] Strikman M 2000 QCD factorization theorems for DIS exclusive processes and inclusive diffraction: new probes of hadrons and nuclei *Nucl. Phys.* A **663** 64c–73c

[165] Miller G A and Strikman M 2010 Color transparency at COMPASS energies *Phys. Rev.* C **82** 025205

[166] Forest J L *et al* 1996 Femtometer toroidal structures in nuclei *Phys. Rev.* C **54** 646–67

[167] Buchanan C D and Yearian M R 1965 Elastic electron–deuteron scattering and possible meson-exchange effects *Phys. Rev. Lett.* **15** 303–6

[168] Elias J E *et al* 1969 Measurements of elastic electron–deuteron scattering at high momentum transfers *Phys. Rev.* **177** 2075–92

[169] Benaksas D, Drickey D and Frerejacque D 1964 Electromagnetic form factors of the deuteron *Phys. Rev. Lett.* **13** 353–5

[170] Benaksas D, Drickey D and Frèrejacque D 1966 Deuteron electromagnetic form factors for 3 $f^{-2} < q^2 < 6\ f^{-2}$ *Phys. Rev.* **148** 1327–31

[171] Arnold R G, Carlson C E and Gross F 1980 Elastic electron–deuteron scattering at high-energy *Phys. Rev.* C **21** 1426

[172] Platchkov S *et al* 1990 Deuteron $A(Q^2)$ structure function and the neutron electric form-factor *Nucl. Phys.* A **510** 740–58

[173] Galster S *et al* 1971 Elastic electron–deuteron scattering and the electric neutron form-factor at four momentum transfers 5 fm$^{-2} < q^2 <$ 14 fm^{-2} *Nucl. Phys.* B **32** 221–37

[174] Cramer R *et al* 1985 Measurement of the magnetic form-factor of the deuteron for $Q^2 = 0.5$ GeV/c^2 to 1.3 GeV/c^2 by a coincidence experiment *Z. Phys.* C **29** 513–18

[175] Simon G G, Schmitt C and Walther V H 1981 Elastic electric and magnetic e d scattering at low momentum transfer *Nucl. Phys.* A **364** 285–96

[176] Abbott D *et al* 1999 A precise measurement of the deuteron elastic structure function $A(Q^2)$ *Phys. Rev. Lett.* **82** 1379–82

[177] Alexa L C *et al* 1999 Large momentum transfer measurements of the deuteron elastic structure function $A(Q^2)$ at Jefferson Laboratory *Phys. Rev. Lett.* **82** 1374–8

[178] Berard R W *et al* 1973 Elastic electron deuteron scattering *Phys. Lett.* B **47** 355–8

[179] Akimov Yu K *et al* 1979 Investigation of elastic electron–deuteron scattering in the region of the squared transfer momentum 0.36-F^{-2}–0.9-F^{-2} *Sov. J. Nucl. Phys.* **29** 335

[180] Bosted P E *et al* 1990 Measurements of the deuteron and proton magnetic form-factors at large momentum transfers *Phys. Rev.* C **42** 38–64

[181] Auffret S *et al* 1985 Magnetic form-factor of the deuteron *Phys. Rev. Lett.* **54** 649–52

[182] Arnold R G *et al* 1987 Deuteron magnetic form-factor measurements at high momentum transfer *Phys. Rev. Lett.* **58** 1723

[183] Schulze M E *et al* 1984 Measurement of the tensor polarization in electron–deuteron elastic scattering *Phys. Rev. Lett.* **52** 597–600

[184] The I *et al* 1991 Measurement of tensor polarization in elastic electron deuteron scattering in the momentum transfer range 3.8 fm$^{-1} \leqslant q \leqslant$ 4.6 fm^{-1} *Phys. Rev. Lett.* **67** 173–6

[185] Garcon M *et al* 1994 Tensor polarization in elastic electron–deuteron scattering in the momentum transfer range 3.8 fm$^{-1} \leqslant q \leqslant$ 4.6 fm^{-1} *Phys. Rev.* C **49** 2516–37

[186] Abbott D *et al* 2000 Measurement of tensor polarization in elastic electron deuteron scattering at large momentum transfer *Phys. Rev. Lett.* **84** 5053–7

[187] Dmitriev V F *et al* 1985 First measurement of the asymmetry in electron scattering by a jet target of polarized deuterium atoms *Phys. Lett.* B **157** 143–5

[188] Voitsekhovsky B B *et al* 1986 Asymmetry in the reaction d(e, e′d) at a momentum transfer of 1 fm^{-1}–1.5 fm^{-1} *JETP Lett.* **43** 733–6

[189] Gilman R *et al* 1990 Measurement of tensor analyzing power in electron deuteron elastic scattering *Phys. Rev. Lett.* **65** 1733–6

[190] Boden B *et al* 1991 Elastic electron deuteron scattering on a tensor polarized solid ND-3 target *Z. Phys.* C **49** 175–86

[191] Ferro-Luzzi M *et al* 1996 Measurement of tensor analyzing powers for elastic electron scattering from a polarized H-2 target internal to a storage ring *Phys. Rev. Lett.* **77** 2630–3

[192] Bouwhuis M *et al* 1999 Measurement of T_{20} in elastic electron deuteron scattering *Phys. Rev. Lett.* **82** 3755–8

[193] Nikolenko D M *et al* 2003 Measurement of the tensor analyzing powers T_{20} and T_{21} in elastic electron deuteron scattering *Phys. Rev. Lett.* **90** 072501

[194] Zhang C *et al* 2011 Precise measurement of deuteron tensor analyzing powers with BLAST *Phys. Rev. Lett.* **107** 252501

[195] Dirac P A M 1949 Forms of relativistic dynamics *Rev. Mod. Phys.* **21** 392–9

[196] Polyzou W N *et al* 2011 Mini review of Poincaré invariant quantum theory *Few Body Syst.* **49** 129–47

[197] Huang Y and Polyzou W N 2009 Exchange current contributions in null-plane quantum models of elastic electron deuteron scattering *Phys. Rev.* C **80** 025503

[198] Bradford R, Bodek A, Budd H S and Arrington J 2006 A new parameterization of the nucleon elastic form-factors *Nucl. Phys. Proc. Suppl.* **159** 127–32

[199] Phillips D R, Wallace S J and Devine N K 2005 Electron–deuteron scattering in the equal-time formalism: beyond the impulse approximation *Phys. Rev.* C **72** 014006

[200] Van Orden J W, Devine N and Gross F 1995 Elastic electron scattering from the deuteron using the gross equation *Phys. Rev. Lett.* **75** 4369–72

[201] Pinto S A, Stadler A and Gross F 2010 First results for electromagnetic three-nucleon form factors from high-precision two-nucleon interactions *Phys. Rev.* C **81** 014007

[202] Gross F and Stadler A 2007 High-precision covariant one-boson-exchange potentials for np scattering below 350 MeV *Phys. Lett.* B **657** 176–9

[203] Gross F and Stadler A 2008 Covariant spectator theory of np scattering: phase shifts obtained from precision fits to data below 350 MeV *Phys. Rev.* C **78** 014005

[204] Tandy P C 1999 Electromagnetic form-factors of meson transitions *Fizika* B **8** 295–302

[205] Landshoff P V and Polkinghorne J C 1973 p p elastic scattering at large momentum transfer *Phys. Lett.* B **44** 293–5

[206] Sivers D W, Brodsky S J and Blankenbecler R 1976 Large transverse momentum processes *Phys. Rep.* **23** 1–121

[207] Khiari F Z *et al* 1989 Acceleration of polarized protons to 22 GeV/c and the measurement of spin–spin effects in $p\uparrow + p\uparrow \rightarrow p + p$ *Phys. Rev.* D **39** 45–85

[208] Crabb D G *et al* 1990 High-precision measurement of the analyzing power in large-$p_\perp^2$ spin-polarized 24 GeV/c proton–proton elastic scattering *Phys. Rev. Lett.* **65** 3241–4

[209] Ralston J P and Pire B 1988 Fluctuating proton size and oscillating color transparency *Phys. Rev. Lett.* **61** 1823–6

[210] Brodsky S J and de Teramond G F 1988 Spin correlations, qcd color transparency, and heavy-quark thresholds in proton–proton scattering *Phys. Rev. Lett.* **60** 1924–7

[211] Farrar G R, Huleihel K and Zhang H 1995 Deuteron form factor *Phys. Rev. Lett.* **74** 650–3

[212] Brodsky S J and Hiller J R 1983 Reduced nuclear amplitudes in quantum chromodynamics *Phys. Rev.* C **28** 475

[213] Carlson C E and Gross F 1984 Distinctive signatures for quantum chromodynamics in nuclear physics *Phys. Rev. Lett.* **53** 127–9

[214] Brodsky S J and Hiller J R 1992 Universal properties of the electromagnetic interactions of spin-one systems *Phys. Rev. D* **46** 2141–9

[215] Kobushkin A and Syamtomov A 1994 High-q^2 elastic ed scattering and QCD predictions *Phys. Rev.* D **49** 1637–8

[216] Cao J and Wu H-F 1997 Light-cone qcd predictions for elastic *ed* scattering in the intermediate energy region *Phys. Rev.* C **55** 2191–5

[217] Carlson C E, Hiller J R and Holt R J 1997 Relativistic QCD view of the deuteron *Ann. Rev. Nucl. Part. Sci.* **47** 395–428

[218] De Forest T and Mulders P J 1987 Effects of quark antisymmetrization in a schematic model of the nucleus *Phys. Rev.* D **35** 2849

[219] Dijk H and Bakker B L G 1989 Multi-quark effects in the singlet s wave and triplet s wave triplet D wave neutron–proton scattering states and the deuteron *Nucl. Phys.* A **494** 438

[220] Robson D 1999 Quark correlations and deuteron electromagnetic form factors *Phys. Rev.* C **61** 015202

[221] Pirner H J and Vary J P 2011 Boundary between hadron and quark/gluon structure of nuclei *Phys. Rev.* C **84** 015201

[222] Higinbotham D W, Piasetzky E, Weinstein L and Wood S A 2011 Short-distance structure of nuclei *J. Phys.: Conf. Ser.* **299** 012010

[223] Julia-Diaz B and Lee T S H 2003 Quark exchange mechanism of γd $\rightarrow$ np reaction at 2 GeV to 6 GeV *Mod. Phys. Lett.* A **18** 200–7

[224] Grishina Yu V *et al* 2003 Polarization observables in high-energy deuteron photodisintegration within the quark gluon strings model *Eur. Phys. J.* A **18** 207–9

[225] Grishina Yu V *et al* 2004 Forward–backward angle asymmetry and polarization observables in high-energy deuteron photodisintegration *Eur. Phys. J.* A **19** 117–23

[226] Mirazita M *et al* 2004 Complete angular distribution measurements of two-body deuteron photodisintegration between 0.5 GeV and 3 GeV *Phys. Rev.* C **70** 014005

[227] Schulte E C *et al* 2002 High energy angular distribution measurements of the exclusive deuteron photodisintegration reaction *Phys. Rev.* C **66** 042201

[228] Rossi P *et al* 2005 Onset of asymptotic scaling in deuteron photodisintegration *Phys. Rev. Lett.* **94** 012301

[229] Schulte E C *et al* 2001 Measurement of the high energy two-body deuteron photodisintegration differential cross-section *Phys. Rev. Lett.* **87** 102302

[230] Rachek I A *et al* 2007 Measurement of tensor analyzing powers in deuteron photodisintegration *Phys. Rev. Lett.* **98** 182303

[231] Schwamb M 2010 Unified description of hadronic and electromagnetic reactions of the two-nucleon system *Phys. Rep.* **485** 109–93

[232] Schwamb M and Arenhovel H 2001 The role of meson retardation in deuteron photodisintegration above pion threshold *Nucl. Phys.* A **690** 682–710

[233] Jiang X *et al* 2007 Recoil-proton polarization in high-energy deuteron photodisintegration with circularly polarized photons *Phys. Rev. Lett.* **98** 182302

[234] Sargsian M M 2004 Polarization observables in hard rescattering mechanism of deuteron photodisintegration *Phys. Lett.* B **587** 41–51

[235] Wijesooriya K *et al* 2001 Polarization measurements in high-energy deuteron photodisintegration *Phys. Rev. Lett.* **86** 2975–9

[236] Khokhlov N A, Knyr V A and Neudatchin V G 2007 Nucleon–nucleon wave function with short-range nodes and high-energy deuteron photodisintegration *Phys. Rev.* C **75** 064001

[237] Glister J *et al* 2011 Polarization observables in deuteron photodisintegration below 360 MeV *Phys. Lett.* B **697** 194–8

[238] Dutta D *et al* 2011 Jefferson Lab LOI-11-103

[239] Granados C G and Sargsian M M 2011 Hard breakup of the deuteron into two delta-isobars *Phys. Rev.* C **83** 054606

[240] Amroun A *et al* 1994 H-3 and He-3 electromagnetic form-factors *Nucl. Phys.* A **579** 596–626

[241] Nakagawa I *et al* 2001 Measurement of the elastic magnetic form factor of ^{3}He at high momentum transfer *Phys. Rev. Lett.* **86** 5446–9

[242] Arnold R G *et al* 1978 Elastic electron scattering from He-3 and He-4 at high momentum transfer *Phys. Rev. Lett.* **40** 1429
[243] Sick I 2001 Elastic electron scattering from light nuclei *Prog. Part. Nucl. Phys.* **47** 245–318
[244] Gomez J *et al* 2004 Jefferson Lab experiment E04-018
[245] Brodsky S J *et al* 2004 Hard photodisintegration of a proton pair in He-3 *Phys. Lett.* B **578** 69–77
[246] Sargsian M M and Granados C 2009 Hard break-up of two-nucleons from the ^{3}He nucleus *Phys. Rev.* C **80** 014612
[247] Granados C 2011 QCD structure of nuclear interactions arXiv:1108:4977 [nucl-th]
[248] Kondratyuk L A *et al* 1993 Deuteron photodisintegration, quark gluon string model and Regge phenomenology *Phys. Rev.* C **48** 2491–7
[249] Frankfurt L L, Miller G A, Sargsian M M and Strikman M I 2000 QCD rescattering and high-energy two-body photodisintegration of the deuteron *Phys. Rev. Lett.* **84** 3045–8
[250] Crawford R *et al* 1996 Two-body photodisintegration of the deuteron from 100 MeV to 800 MeV *Nucl. Phys.* A **603** 303–25
[251] Napolitano J *et al* 1988 Measurement of the differential cross-section for the reaction ^{2}H(γ, p)n at high photon energies and $\theta_{\mathrm{c.m.}} = 90^\circ$ *Phys. Rev. Lett.* **61** 2530–3
[252] Freedman S J *et al* 1993 Two-body disintegration of the deuteron with 0.8 GeV to 1.8 GeV photons *Phys. Rev.* C **48** 1864–78
[253] Belz J E *et al* 1995 Two body photodisintegration of the deuteron up to 2.8 GeV *Phys. Rev. Lett.* **74** 646–9
[254] Bochna C *et al* 1998 Measurements of deuteron photodisintegration up to 4.0 GeV *Phys. Rev. Lett.* **81** 4576–9
[255] Pomerantz I *et al* 2010 Hard photodisintegration of a proton pair *Phys. Lett.* B **684** 106–9
[256] Niccolai S *et al* 2004 Complete measurement of three-body photodisintegration of He-3 for photon energies between 0.35 GeV and 1.55 GeV *Phys. Rev.* C **70** 064003
[257] Nasseripour R *et al* 2009 Photodisintegration of ^{4}He into p + t *Phys. Rev.* C **80** 044603
[258] Pomerantz I *et al* 2011 unpublished